Mon. Not. R. Astron. Soc. **000**, 000–000 (0000) Printed 5 February 2008 (MN LATEX style file v2.2)

The mass distribution in early-type disk galaxies: declining rotation curves and correlations with optical properties

E. Noordermeer,[1,2⋆] J. M. van der Hulst,[1] R. Sancisi,[1,3] R. S. Swaters[4] and T. S. van Albada[1]

[1] *Kapteyn Astronomical Institute, University of Groningen, PO Box 800, 9700 AV Groningen, The Netherlands*
[2] *University of Nottingham, School of Physics and Astronomy, University Park, NG7 2RD Nottingham, UK*
[3] *INAF-Osservatorio Astronomico di Bologna, Via Ranzani 1, 40127 Bologna, Italy*
[4] *Department of Astronomy, University of Maryland, College Park, MD 20742-2421, USA*

accepted for publication in MNRAS, 05-01-2007

ABSTRACT

We present rotation curves for 19 early-type disk galaxies (S0 – Sab). The galaxies span a B-band absolute magnitude range from −17.5 to −22, but the majority have a high luminosity with $M_B < -20$. Rotation velocities are measured from a combination of HI velocity fields and long-slit optical emission line spectra along the major axis; the resulting rotation curves probe the gravitational potential on scales ranging from 100 pc to 100 kpc.

We find that the rotation curves generally rise rapidly in the central regions and often reach rotation velocities of 200 – 300 km/s within a few hundred parsecs of the centre. The detailed shape of the central rotation curves shows a clear dependence on the concentration of the stellar light distribution and the bulge-to-disk luminosity ratio: galaxies with highly concentrated stellar light distributions reach the maximum in their rotation curves at relatively smaller radii than galaxies with small bulges and a relatively diffuse light distribution. We interpret this as a strong indication that the dynamics in the central regions are dominated by the stellar mass.

At intermediate radii, many rotation curves decline, with the asymptotic rotation velocity typically 10 – 20% lower than the maximum. The strength of the decline is correlated with the total luminosity of the galaxies, more luminous galaxies having on average more strongly declining rotation curves. At large radii, however, all declining rotation curves flatten out, indicating that substantial amounts of dark matter must be present in these galaxies too.

A comparison of our rotation curves with the Universal Rotation Curve from Persic et al. (1996) reveals large discrepancies between the observed and predicted rotation curves; we argue that rotation curves form a multi-parameter family which is too complex to describe with a simple formula depending on total luminosity only.

In a number of galaxies from our sample, there is evidence for the presence of rapidly rotating gas in the inner few hundred parsecs from the centers. The inferred central masses and mass densities are too high to be explained by the observed stellar components and suggest the presence of supermassive black holes in these galaxies.

Key words: galaxies: spiral – galaxies: lenticular – galaxies: structure – galaxies: fundamental parameters – galaxies: kinematics and dynamics – galaxies: haloes

1 INTRODUCTION

Rotation curves are the prime tool for studying the mass distribution in disk galaxies. In normal, unperturbed galaxies, gas moves on circular orbits around the centre, so measurements of the circular velocity can be used to yield the enclosed mass at different radii. The study of the shapes of rotation curves therefore gives important insight into the overall distribution of mass in disk galaxies. HI rotation curves in particular are useful, because they probe the mass distribution to much larger radii than can be achieved with optical data and reach to the regions where dark matter dominates the gravitational potential. In fact, it was the discovery, first made in the 1970's (Rogstad & Shostak 1972;

⋆ email:edo.noordermeer@nottingham.ac.uk

Roberts & Whitehurst 1975; Bosma 1978; Bosma 1981), that HI rotation curves stay flat till the last measured points, well outside the optical disk, which gave the final, irrefutable evidence of the presence of large amounts of unseen matter in galaxies (Bosma 1981; van Albada et al. 1985; van Albada & Sancisi 1986; Begeman 1987).

A long standing question concerns the relation between the shape of rotation curves and other properties of individual galaxies. It has been known for a long time that the shape of a rotation curve is strongly coupled to the optical luminosity of a galaxy: slowly rising and low amplitude for low-luminosity galaxies, high central gradient and high rotation velocities for high-luminosity systems (e.g. Rubin et al. 1985; Burstein & Rubin 1985). However, the question of whether or not other optical properties influence rotation curves as well has resulted in inconsistent answers. Rubin et al. (1985) and Burstein & Rubin (1985) found no dependence on morphological type or on the shape of the light distribution (notably the bulge-to-disk ratio) and presented synthetic rotation curves depending solely on a galaxy's luminosity. This idea was later elaborated by Persic & Salucci (1991) and Persic et al. (1996), who presented a 'universal rotation curve', an analytic formula describing the shape of a rotation curve which only depends on total luminosity.

In contrast, several other studies suggested that rotation curve shape is not correlated with luminosity only, but that other parameters need to be taken into account as well. Corradi & Capaccioli (1990) found that the shape of a rotation curve correlates with a galaxy's morphological type: early-type spirals with large bulges have rotation curves which rise more rapidly than galaxies of similar luminosity but with a less concentrated light distribution. Casertano & van Gorkom (1991) showed that the outer shape of rotation curves is correlated with both the total luminosity and the shape of the light distribution, exemplified by two luminous galaxies with highly concentrated light distributions which have declining rotation curves. Roscoe (1999) showed that the universal rotation curve formalism of Persic et al. (1996) can be improved by including surface brightness as parameter influencing rotation curve shape. The dependence of rotation curve shape on the optical characteristics was also confirmed in studies by e.g. Broeils (1992), Swaters (1999), Verheijen (2001), Matthews & Gallagher (2002) and Sancisi (2004).

The systematics behind rotation curve shapes hold important clues on the structure and evolution of (disk) galaxies. Rubin et al. (1985) and Burstein & Rubin (1985) interpreted the lack of dependence on the light distribution as evidence that luminous matter plays a minor rôle dynamically, and that large amounts of dark matter must be present everywhere in disk galaxies. But if rotation curves are, instead, a multi-parameter family depending also on properties such as morphological type, surface brightness, etc., then the conclusion must be that at least in some galaxies, the stars contribute significantly to the potential. The rotation curve vs. optical properties relations also provide a powerful benchmark for simulations of galaxy formation: any viable theory of galaxy formation must be able to reproduce realistic rotation curves which match the other characteristics of the simulated galaxy.

In order to obtain a better understanding of these issues, a systematic study of HI rotation curves in spiral galaxies, covering a large range of luminosities, morphological types and surface brightnesses, is a crucial step. Although much work has been done in this field in recent years (e.g. de Blok et al. 1996; Swaters 1999; Côté et al. 2000; Verheijen 2001; Gentile et al. 2004), most studies have focused on late-type and low-luminosity galaxies. Early-type disk galaxies, which generally contain less gas (Roberts & Haynes 1994; Noordermeer et al. 2005), have received considerably less attention. One of the few studies so far aimed at a systematic investigation of HI rotation curves over the full range of morphological types was that by Broeils (1992). However, in his sample of 23 galaxies, only one was of morphological type earlier than Sb and only four had $V_{\rm max} > 250\,{\rm km\,s^{-1}}$. The only large-scale HI survey directed specifically at S0 and Sa galaxies was carried out by van Driel (1987), but his study was severely hampered by the low signal-to-noise ratio of his data and his rotation curves were of rather poor quality compared to modern standards. In the optical, little work has been done on early-type spiral galaxies either, since the early studies by Rubin et al. (1985) and Kent (1988). S0 and Sa galaxies were thus also under-represented in the study by Persic et al. (1996); their Universal Rotation Curve is based on over 1000 rotation curves of which only 2 are of type Sab or earlier.

This paper is part of a larger study designed to fill this lack and to systematically investigate the relation between dark and luminous matter in early-type disk galaxies. These systems, lying at the high mass, high surface brightness end of the disk galaxy population, are ideal test cases to investigate what determines the shape of rotation curves. If the stars contribute significantly to the gravitational potentials of galaxies, it is in these galaxies that their influence will be most easily detected. In an earlier paper (Noordermeer et al. 2005, hereafter paper I), we have presented HI observations for a sample of early-type (S0 – Sab) disk galaxies, and in an accompanying paper to the present one (Noordermeer & van der Hulst 2006, paper II) we present optical photometry and bulge-disk decompositions. Here, we use the data for a subset of 19 galaxies from Paper I to derive their rotation curves and to study the dependence of their rotation curve shapes on the optical properties. In two future publications, we will use the results to study the location of massive, early-type disk galaxies on the Tully-Fisher relation and to create detailed mass-models.

The HI data from Paper I can be used to measure the rotation velocities of the gas out to large radii. In the central regions, however, the rotation curves can often not be measured from the 21cm observations due to the presence of holes in the HI disks (see Paper I). Furthermore, the spatial resolution of our HI observations is usually insufficient to obtain detailed information on the shape of the rotation curves in the inner regions, where our velocity fields suffer from beam smearing. To overcome these difficulties, we use long-slit optical spectroscopy to measure the central rotation curves. In most galaxies, optical emission lines can be detected in the very inner regions, out to radii where reliable rotation velocities can be determined from the HI velocity fields. Moreover, due to the higher spatial resolution of the optical observations, the effects of beam smearing are strongly reduced.

The remainder of this paper is structured as follows.

Table 1. Sample galaxies: basic data. (1) sample number; (2) UGC number; (3) alternative name; (4) morphological type; (5) distance; (6) and (7) absolute B- and R-band magnitudes (corrected for Galactic foreground extinction); (8) R-band central disk surface brightness (corrected for Galactic foreground extinction and inclination effects) and (9) R-band disk scale length. Column (4) was taken from NED, (5) from Paper I and (6) – (9) from Paper II.

sample number	UGC	alternative name	Type	D	M_B	M_R	$\mu^c_{0,R}$	h_R
				Mpc	mag	mag	$\frac{\text{mag}}{\text{arcsec}^2}$	kpc
(1)	(2)	(3)	(4)	(5)	(6)	(7)	(8)	(9)
1	624	NGC 338	Sab	65.1	-20.83	-22.25	21.92	5.8
2	2487	NGC 1167	SA0-	67.4	-21.88	-23.24	20.12	8.0
3	2916	–	Sab	63.5	-21.05	-22.01	20.99	5.0
4	2953	IC 356	SA(s)ab pec	15.1	-21.22	-22.54	19.25	4.1
5	3205	–	Sab	48.7	-20.89	-21.88	19.59	3.5
6	3546	NGC 2273	SB(r)a	27.3	-20.02	-21.35	19.49	2.8
7	3580	–	SA(s)a pec:	19.2	-18.31	-19.42	21.58	2.4
8	3993	–	S0?	61.9	-20.19	-21.35	22.37	5.5
9	4458	NGC 2599	SAa	64.2	-21.38	-22.61	21.26	8.6
10	4605	NGC 2654	SBab: sp	20.9	-20.09†	–†	–†	–†
11	5253	NGC 2985	(R')SA(rs)ab	21.1	-20.86	-21.90	21.32	5.3
12	6786	NGC 3900	SA(r)0+	25.9	-19.94†	-21.13	19.30	1.5
13	6787	NGC 3898	SA(s)ab	18.9	-20.00	-21.28	20.49	3.3
14	8699	NGC 5289	(R)SABab:	36.7	-19.48	-20.74	22.24	3.7
15	9133	NGC 5533	SA(rs)ab	54.3	-21.22	-22.62	21.27	9.1
16	11670	NGC 7013	SA(r)0/a	12.7	-19.20	-20.55	19.58	1.8
17	11852	–	SBa?	80.0	-20.44	-21.53	20.74	4.5
18	11914	NGC 7217	(R)SA(r)ab	14.9	-20.27	-21.35	19.91	2.7
19	12043	NGC 7286	S0/a	15.4	-17.53	-18.26	19.90	0.8

† No data available in Paper II; M_B taken from LEDA.

In section 2, the criteria which were used to select suitable galaxies from the parent sample of Paper I are described. Section 3 describes the techniques that were used to derive the rotation curves from the HI velocity fields and from the optical spectra. In section 4, the fitted orientation parameters and systemic velocities of our galaxies, as derived from different sources, are compared. In section 5, we briefly discuss the occurrence of warps in the galaxies in our sample. In section 6, several aspects of the shape of our rotation curves are discussed, including an analysis of the correlations with optical properties and the applicability of the concept of a 'Universal Rotation Curve' to our data. Finally, we briefly discuss our results and summarize the main conclusions in section 7. In the appendices, we present some additional material. A detailed description of the individual rotation curves is presented in appendix A. In appendix B, we interpret the broad central velocity profiles which are present in some of our optical spectra. Appendix C gives the graphical representation of the rotation curves and various other data for the galaxies in our sample.

2 SAMPLE SELECTION

The galaxies for the rotation curve study presented here were selected from the 68 galaxies with HI observations presented in Paper I, which were in turn selected from the WHISP survey (Westerbork survey of HI in spiral and irregular galaxies; Kamphuis et al. 1996; van der Hulst et al. 2001). In order to be able to derive high quality HI rotation curves, galaxies were selected on the basis of the following criteria: *1*) the velocity field must be well resolved ($> 5-10$ beams across) and defined over significant parts of the gas disks (i.e. not confined to small 'patches'); *2*) the gas must be moving in regular circular orbits around the centre of the galaxy. Strongly interacting galaxies, or galaxies with otherwise distorted kinematics cannot be used. Strongly barred galaxies are excluded as well, because non-circular motions in the bar potential complicate the analysis of the data; *3*) the inclination angle must be well constrained and preferably lie between 40°and 80°.

Few galaxies from Paper I satisfy all these conditions and a strict application of these criteria (especially the second one) would lead to a very small sample. We have therefore relaxed the latter two selection criteria and included a number of galaxies with e.g. weak bars, mild kinematical distortions or a more face- or edge-on orientation. The resulting sample consists of 19 galaxies; a few basic characteristics of the members are given in table 1.

The galaxies in our sample have morphological types ranging from S0- to Sab and span two decades in optical luminosity ($-17.5 > M_B > -22$). The majority of galaxies in our sample have high optical luminosity, with $M_B < -20$. See Paper I for a more detailed description of the properties of the galaxies in our sample.

3 OBSERVATIONS, DATA REDUCTION AND THE DERIVATION OF THE ROTATION CURVES

As mentioned in the introduction, the rotation curves in this paper were derived from a combination of HI synthesis observations and long-slit optical spectra. Below, we discuss the analysis of both components separately.

Table 2. Dynamical properties: (1) UGC number; (2) and (3) position of the dynamical centre; (4) heliocentric systemic velocity; (5) position angle (north through east) of major axis; (6) inclination angle; (7) maximum rotation velocity; (8) rotation velocity at 2.2 R-band disk scale lengths; (9) asymptotic rotation velocities at large radii; (10) total enclosed mass within last measured point and (11) rotation curve quality.

UGC	dynamical centre						$V_{\rm sys}$	PA	i	$V_{\rm max}$	$V_{\rm 2.2h}$	$V_{\rm asymp}$	$M_{\rm enc}$	quality
	RA (2000)			Dec (2000)										
	h	m	s	$^\circ$	$'$	$''$	km/s	$^\circ$		km/s	km/s	km/s	$M_\odot$	
(1)	(2)			(3)			(4)	(5)	(6)	(7)	(8)	(9)	(10)	(11)
624	1	0	36.0	30	40	10	4789	288	64†	300	300	270	$5.2 \cdot 10^{11}$	III
2487	3	1	42.7	35	12	21	4952	250–256	36	390	360	330	$2.1 \cdot 10^{12}$	I
2916	4	2	33.5	71	42	19	4537	242	42–50	220	210	180	$2.8 \cdot 10^{11}$	II
2953	4	7	46.8	69	48	46	892	98–104	50	315	315	260	$1.1 \cdot 10^{12}$	I
3205	4	56	14.9	30	3	8	3586	230–224	67	240	230	210	$4.3 \cdot 10^{11}$	I
3546	6	50	8.6	60	50	46	1837	56	55	260	185	190	$2.4 \cdot 10^{11}$	II
3580	6	55	31.2	69	33	54	1203	6–356	63	127	100	125	$9.0 \cdot 10^{10}$	II
3993	7	55	44	84	55	33	4364	220	20	300	290	250	$8.6 \cdot 10^{11}$	II
4458	8	32	11.2	22	33	36	4756	288–295	25	490	280	240	$7.8 \cdot 10^{11}$	II
4605	8	49	11.1	60	13	14	1347	240–247	84–74	225	220*	185	$2.8 \cdot 10^{11}$	I
5253	9	50	22.2	72	16	44	1329	356–340	37	255	245	210	$5.5 \cdot 10^{11}$	II
6786	11	49	9.2	27	1	15	1795	181–186	68–64	230	–$^\$$	215	$3.1 \cdot 10^{11}$	I
6787	11	49	15.3	56	5	5	1172	107–118	69–66	270	250	250	$5.0 \cdot 10^{11}$	I
8699	13	45	7.7	41	30	19	2516	280	73	205	190	180	$1.9 \cdot 10^{11}$	I
9133	14	16	7.7	35	20	37	3858	24–45	53	300	265	225	$1.3 \cdot 10^{12}$	I
11670	21	3	33.5	29	53	50	774	336–330	70–68	190	155	160	$1.6 \cdot 10^{11}$	II
11852	21	55	59.6	27	53	55	5843	200–175	50–60	220	210	165	$5.9 \cdot 10^{11}$	II
11914	22	7	52.3	31	21	36	951	265–268	31	305	300	300$^\#$	$1.9 \cdot 10^{11}$	II
12043	22	27	50.4	29	5	45	1007	97–92	67	93	82	90	$3.2 \cdot 10^{10}$	I

† Kinematical inclination poorly constrained by observations. Value copied from optical isophotal analysis.
* No accurate photometry available due to edge-on orientation of optical disk; optical scale length is estimate only.
$^\$$ Galaxy does not have regular exponential disk; no optical scale length available.
$^\#$ Rotation curve extends out to 3.3 R disk scale lengths only and may converge to different velocity at larger radii.

3.1 HI rotation curves

The HI rotation curves were derived by fitting tilted ring models (Begeman 1987; Begeman 1989) to the observed velocity fields from Paper I, using the ROTCUR algorithm implemented in GIPSY (Groningen Image Processing System; Vogelaar & Terlouw 2001)[1]. In Paper I, we showed velocity fields at either full ($\approx 15''$), $30''$ or $60''$ resolution. Here, we fit tilted ring models to the velocity fields at all available resolutions. The higher-resolution velocity fields can be used for the inner regions, whereas the velocity fields at lower resolution generally extend out to larger radii and can be used to obtain information about the rotation curves in the outer parts. Tilted rings were fitted to the entire velocity fields, but points near the major axis were given more weight than those near the minor axis by applying a $|\cos(\alpha)|$ weighing scheme, with α the azimuthal angle, measured from the major axis in the plane of the galaxy.

In all cases, the rotation curves were determined in four steps. In the first step, all parameters (i.e. systemic velocity $V_{\rm sys}$, dynamical centre position (x_c, y_c), position angle PA, inclination angle i and rotation velocity $V_{\rm rot}$) were left free for each ring. In general, the fitted systemic velocities and dynamical centre positions show little variation with radius, especially in the inner regions, and the average values were adopted as the global values for the galaxy. They are listed in table 2.

[1] For two highly inclined galaxies, UGC 4605 and 8699, the standard tilted ring method is not suitable and a modified analysis was applied (see individual notes in appendix A).

In the second step, the systemic velocity and dynamical centre were fixed for each ring at the values derived in the first step. The values for the position angle derived from this step are shown with the data points in the figures in appendix C. The position angle is usually well-defined, but it often shows variations with radius as a result of warps in the gas disk. If a clear trend was visible, we fitted it by hand and used the fitted values for the next steps; otherwise we used the average of all rings. The adopted range of position angles, or the average value, for each galaxy is given in table 2, and plotted as bold line in the figures in appendix C.

In the third step, only the inclination and rotation velocity were left as free parameters for each ring. From this fit, the inclination angle was determined. This parameter is the most difficult one to constrain, because it is strongly coupled to the rotation velocity, especially for inclinations lower than $\approx 45^\circ$ (Begeman 1987; Begeman 1989). The fitted values are shown in the figures in appendix C. It is clear that for the more face-on galaxies, the uncertainties in the fitted inclinations are large. In practice, radial variations in inclination could only be detected for galaxies that are sufficiently inclined; for galaxies with $i \lesssim 45^\circ$ only an average value could be determined. When necessary, the fitted inclination angles were also compared to the values derived from the optical images (see Paper II) to make a more reliable estimate. The range of inclination angles, or the average value, used for the next step is given in table 2 and plotted as bold line in the figures in appendix C.

The uncertainty in the inclination $\Delta i(r)$ was estimated by eye, based on the spread of the individual data points around the fitted values and the comparison between the

Table 3. Observational parameters for optical spectroscopic observations: (1) UGC number; (2) telescope used: Isaac Newton Telescope (INT) or William Herschel Telescope (WHT) on La Palma or NOAO 2.1m telescope on Kitt Peak (KP 2.1m); (3) observing dates; (4) total exposure time; (5) and (6) effective slit width and length; (7) position angle (north through east) of the slit on the sky and (8) – (12) line weights used in the stacking procedure.

UGC	telescope	dates	t_{exp}	slit orientation			line weights w_i				
				width	length	PA	[NII]$_{6548}$	Hα	[NII]$_{6583}$	[SII]$_{6716}$	[SII]$_{6731}$
			sec	$''$	$'$	$^\circ$					
(1)	(2)	(3)	(4)	(5)	(6)	(7)	(8)	(9)	(10)	(11)	(12)
624	INT	26/1/01	2400	1.5	3.3	106	0.5	2.0	1.0	0.5	0.5
2487	INT	28/1/01	7200	1.0	3.3	70	0.5	1.0	1.0	0.5	0.5
2916	INT	27/1/01	2400	1.0	3.0	76	0.0	1.0	1.0	0.0	0.0
2953	WHT	2/1/00	7200	1.0	4.0	99	0.5	1.0	1.0	0.5	0.5
3205	INT	26/1/01	6000	1.5	3.3	47	0.0	1.0	1.0	0.0	0.0
3546	INT	26/1/01	3600	1.5	3.3	57	0.0	1.0	2.0	0.0	0.0
3580	INT	28/1/01	3600	1.0	3.3	5	0.25	1.0	0.5	0.5	0.5
3993	INT	26/1/01	7200	1.5	3.0	44	0.25	0.5	1.0	0.5	0.5
4458	INT	27/1/01	3600	1.0	3.0	100	0.25	1.0	1.0	0.25	0.25
4605	INT	28/1/01	4800	1.0	3.3	63	0.0	2.0	1.0	0.5	0.5
5253	INT	27/1/01	2400	1.0	3.2	0	0.1	1.0	1.0	0.3	0.3
6786	INT	29/1/01	2400	1.0	3.3	2	0.0	1.0†	1.0†	0.0	0.0
6787	INT	31/1/01	6000	1.0	3.3	105	0.1	1.0	0.5	0.25	0.25
8699	INT	22/5/01	3600	1.0	3.6	100	0.25	1.0	1.0	0.5	0.5
9133	INT	22/5/01	7200	1.0	3.6	27	0.0	1.0	1.0	0.0	0.0
11670	INT	22/5/01	4200	1.0	3.6	157	0.25	1.0	1.0	0.5	0.5
11852	INT	23/5/01	4800	1.0	3.6	15	0.0	1.0	1.0	0.0	0.0
11914	INT	23/5/01	3150	1.0	3.6	89	0.25	1.0	1.0	0.25	0.25
12043	KP 2.1m	8/12/01	2400	1.0	5.2	98	0.25	2.0	0.5	0.7	0.0

† Lines could not be stacked because of stellar absorption feature in Hα (see note in appendix A).

tilted ring inclination angles and optical ellipticity. In general, we let the uncertainty Δi increase with radius, in order to account for the possibility of undetected or misfitted warps in the outer gas disks of the galaxies. The adopted uncertainties in the inclination angle are shown with the shaded regions in the bottom middle panels in the figures in appendix C.

In the final step, we derived the rotation curves by doing a fit with all parameters fixed except the rotation velocity. To prevent the inclusion of erroneous points in the final rotation curves, outer tilted rings were not accepted if they only covered a small number of pixels in the velocity field, or if the outer parts of the velocity fields showed clear signs of non-circular or otherwise perturbed motions. The final HI rotation curves are shown as square data points in the bottom right panels in the figures in appendix C.

3.2 Rotation curves from optical spectra

3.2.1 observations

For most galaxies in the sample, long-slit spectra were taken with the IDS spectrograph on the Isaac Newton Telescope (INT) on La Palma[2]. For UGC 2953, a spectrum was obtained from the red arm of the ISIS spectrograph on the William Herschel Telescope, also on La Palma[2]. The spectrum of UGC 12043 was taken with the GoldCam spectrograph, mounted on the NOAO 2.1m telescope on Kitt Peak, Arizona[3]. A summary of the observations is given in table 3.

The slits of the spectrographs were aligned with the major axes of the galaxies. In some cases, the position angle of the slit on the sky was slightly different from the kinematical position angle of the galaxy as derived from the HI velocity field. In these cases, the rotation curves were later corrected for the effect of the misalignment. The bulges of the galaxies were usually bright enough to enable the slit to be positioned accurately over the centres using the TV camera in the focal plane.

The spectral range of all observations was chosen such that each spectrum contains the redshifted lines of Hα ($\lambda_0 =$ 6562.80 Å), [NII] (6548.04 and 6583.46 Å) and [SII] (6716.44 and 6730.81 Å). The spectral resolution of the spectra taken on the INT is 1.0 and 1.4 Å (FWHM) for slit widths of 1.0 and 1.5$''$ respectively, corresponding to a velocity resolution of approximately 45 and 65 km/s respectively. The spectrum for UGC 2953 has a spectral resolution of 0.9 Å ($\sim$ 40 km/s), whereas the resolution of the spectrum for UGC 12043 is slightly worse at 2.0 Å ($\sim$ 90 km/s).

Total exposure times were broken up into single exposures of typically 20 minutes; the number of exposures for each galaxy was determined at the telescope, based on the strength of the emission lines in the first exposure.

[2] The Isaac Newton Telescope and William Herschel Telescope are operated on the island of La Palma by the Isaac Newton Group in the Spanish Observatorio del Roque de los Muchachos of the Instituto de Astrofisica de Canarias.

[3] The Kitt Peak 2.1m telescope is operated and IRAF is distributed by the National Optical Astronomy Observatories, which are operated by the Association of Universities for Research in Astronomy, Inc., under cooperative agreement with the National Science Foundation.

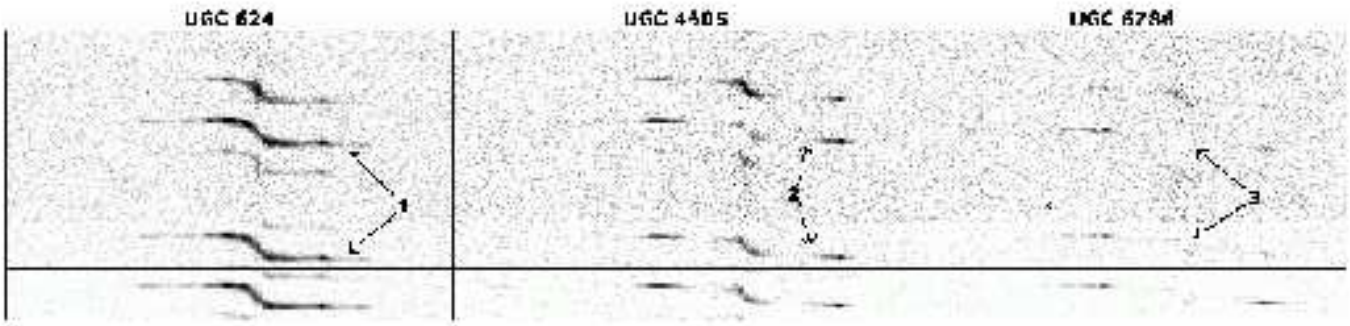

Figure 1. Example spectra to illustrate the spectral stacking procedure. The top panel at each column shows a section of the original spectrum, centered around the Hα- (middle) and the 6583 and 6548 Å [NII]-lines (top and bottom respectively), after removal of the stellar continuum and sky lines. The middle panels show the stacked spectra, where the emission from all lines (including the [SII]-lines) is added, with weights w_i as given in table 3. The bottom panels show the same spectra after binning along the spatial direction to $\sim 1''$ pixels. For each galaxy, the 3 spectra are shown on the same (logarithmic) intensity scale, to show the decrease in the noise levels between the subsequent steps. The arrows refer to specific features in the spectra and are discussed in the text.

3.2.2 data reduction

Standard data reduction steps were performed within the IRAF environment[3]. Readout bias was subtracted using the overscan region of the chips; any remaining structure was removed using special bias frames. The spectra were then flatfielded using Tungsten flatfields. Wavelength calibrations were performed using arc spectra from Copper, Neon and Argon lamps, taken before or after the galaxy spectra. The resulting wavelength solutions were used to map the spectra to a logarithmic wavelength grid, such that pixel shifts correspond to linear velocity shifts. The calibrations were also checked retrospectively by comparing the measured wavelengths of a few strong night-sky lines with the values given by Osterbrock et al. (1996); the systematic errors lie typically in the range 0.05 – 0.10 Å, corresponding to about 2.5 – 5 km/s.

Individual exposures were then combined and cosmic rays were rejected using a simple sigma-clipping criterion. The continuum emission of the galaxy and the night-sky emission lines were removed by fitting low-order polynomials along the spectral and spatial axes of the spectra respectively.

In the final, cleaned spectra, the Hα line is usually the strongest line in the outer parts of the galaxies. In the central parts however, the 6583.46 Å [NII] line and the [SII] lines are often stronger, presumably due to underlying stellar absorption in Hα. Rather than first determining rotation curves for each line separately and then combining them into one single curve, we have chosen the reverse order. The parts of the spectrum around each of the 5 emission lines were shifted according to the difference in rest wavelength and stacked to create a single spectrum which contains emission from all lines. Each line was roughly weighted according to its relative strength; the weights w_i are given in table 3. Before stacking, special care was taken to ensure that the different emission lines trace similar velocities, but we found no cases with significant differences. This procedure has the added advantage that the signal-to-noise ratio in the stacked spectrum is higher than in the original one; emission that was too weak to be detected in each line individually could sometimes be detected with sufficient significance in the stacked spectrum.

In figure 1, we illustrate the stacking procedure for three representative galaxies. In the spectrum of UGC 624 (*left*), the Hα line is the strongest line along the entire slit, but adding the other lines leads to a slightly higher signal-to-noise ratio (see for example the location indicated with arrows 1), and thus improves the accuracy of the fitted velocities. For UGC 4605 (*middle*), the improvement is more significant. In the original spectrum, Hα is stronger in the outer parts, but the 6583.46 Å [NII]-line is stronger in the centre. In the stacked spectrum, velocities can be measured in both regions, as well as at locations where the signal in the individual lines was too weak to be fitted (arrows 2). For UGC 6786 (*right*), the stacking procedure does not work due to a strong stellar Hα absorption feature in the centre (arrow 3). In this case, stacking the various lines causes the Hα absorption feature to dilute the little emission that is present in the 6583.46 Å [NII]-line, and thus degrades, rather than improves, the quality of the data. In this case, we analysed both lines separately, and combined the resulting rotation curves afterwards (see also the note in appendix A).

The final cleaned and stacked spectra are shown in the top middle panels in the figures in appendix C.

3.2.3 derivation of the rotation curves

From the stacked spectra, the radial velocity of the emitting gas was determined at each position along the slit by fitting Gaussian profiles along the wavelength direction. Before performing the fits, the spectra were binned in the spatial direction to $\sim 1-2''$ pixels to increase the signal-to-noise ratio of the data and to ensure that only one data point is fitted per resolution element. In some cases, parts of the spectra had such low-level emission that the signal-to-noise ratio was still too low in the binned spectra; for those regions, larger bin sizes were used. Spurious fits or fits with very large errorbars were discarded by hand. The fitted velocities are shown overplotted over the binned spectra in the top middle panels in the figures in appendix C. They are also overplotted over a major-axis slice through the HI data cube, shown in the top right panels in the same figures.

The radial velocity curves for the approaching and receding sides were then folded, using the centre of the optical continuum emission as central position. In two cases, UGC 3205 and 3580, the centres of symmetry of the emis-

sion lines appear shifted with respect to the location of the brightest continuum emission, in both cases by approximately one arcsecond (see the figures in appendix C). In these two cases, we determined by eye the central position which gave the largest degree of symmetry in the folded rotation curves. In the case of UGC 3580, the offset can easily be explained as a result of absorption of continuum emission by dust (see appendix A); for UGC 3205, the origin of the offset is unknown.

The systemic velocity was determined by taking, at each radius, the midpoint of the velocities of the approaching and receding sides and taking the average of the resulting values. This procedure maximizes the symmetry between the approaching and receding sides of the rotation curves over the full length of the spectra. In most cases, the systemic velocity thus derived is consistent with the value found from the HI data (see also figure 2). In some cases, small differences were found; this happened mostly in galaxies which are kinematically lopsided, where an unambiguous determination of the systemic velocity is difficult. In those cases, we closely inspected the optical spectrum and the HI velocity fields and determined interactively the systemic velocity which led to the smallest asymmetry in the final, combined optical and HI rotation curves.

Finally, the radial velocity relative to the systemic velocity was calculated for each point and, at radii where emission was detected on both sides of the galaxy, the weighted average was determined. The final rotation curves were subsequently derived by correcting the average radial velocity curves for the inclination of the galaxy and for possible misalignments of the slit with the true major axis; the values for the inclination and position angle were taken from the results of the tilted ring fits to the HI velocity fields, described above. The resulting rotation velocities are shown with the filled circles in the bottom right panels in the figures in appendix C.

3.2.4 optical beam smearing and other line-of-sight integration effects

Close inspection of the optical spectra reveals that in many cases, the rotation curves rise so steeply in the centres of the galaxies that even in the optical spectra, the gradients are not fully resolved. Thus, although the optical spectra are a major improvement over the lower resolution of the HI observations, they suffer from the optical equivalent of beam smearing as well and the fitted velocities in the central parts may still not represent the actual rotation velocities.

Furthermore, many spectra have line profiles that are broadened even at positions several arcseconds away from the centres of the galaxies, where lack of resolution is not expected to play a major role anymore. These broadened profiles may be the result of line-of-sight integration effects through the disks and bulges of the galaxies. Again, the simple Gaussians which were fitted to these line profiles will not recover the true radial velocity at the projected radius and cannot be used for the final rotation curves.

We have adopted a method similar to the envelope-tracing (or terminal velocity) technique (Sancisi & Allen 1979; Sofue 1996; García-Ruiz et al. 2002) to correct the inner points of the optical rotation curves which are affected by optical beam smearing and/or other line-of-sight integration effects. We determined by eye the terminal velocities of the affected line profiles, taking into account the instrumental velocity resolution. The effect of random motions of the emitting gas clouds is ignored, as it is generally much smaller than the instrumental broadening of the profiles ($\sim$10 vs. $\sim$50 km/s). The radial velocities that were thus derived were then processed in the same way as the results from the Gauss fits to derive the average inner rotation curve. The resulting rotation velocities are shown with the open circles in the figures in appendix C.

Although the manually corrected rotation velocities are certainly a better approximation of the true velocities than the results of simple Gauss fits to the line profiles, there are many uncertainties, particularly regarding the detailed 3D distribution of the gas, that cannot be accounted for with the data used here. A more rigorous investigation of the kinematics in the central parts of the galaxies studied here would require even higher spatial resolution and preferably a fully 2D velocity field, i.e. either space-based or adaptive-optics assisted integral field spectroscopic observations.

3.3 Final steps

For the final rotation curves, the output from the tilted ring fits to the HI velocity fields was compared to the derived optical rotation curves and it was determined which HI data points were affected by beam smearing. Central HI data points which lay significantly below the optical velocities were discarded. In almost all cases, the effect of beam smearing was limited to 1 – 2 HI beam sizes from the centre, and only the inner two or three points of the HI rotation curves had to be rejected. Only in highly inclined galaxies, such as UGC 4605 or 8699, do beam smearing and line-of-sight integration effects play a role at larger radii; these galaxies were treated individually to ensure that optimal corrections were applied (see appendix A). Outside the regions where the HI observations are affected by beam smearing, the optical and HI rotation curves generally agree to a high degree ($\lesssim$ 10 km/s).

The remaining HI data points were then combined with the optical data to produce the final rotation curves. Our final curves probe the rotation velocities over 2 – 3 decades of radii and enable us to measure small scale variations in the inner parts of the optical disks as well as the behaviour in the outer parts of the gas disks, many optical scale lengths away from the centre.

The combined data points and their corresponding errors can be used, without further manipulation, to fit detailed mass models and to study the distribution of luminous and dark matter in the galaxies; this will be done in a forthcoming publication. For the remainder of this paper, we are interested mainly in the global properties and shapes of the rotation curves. For this purpose, it is helpful to remove the statistical fluctuations between the individual data points, especially those from the optical spectra. To do so, we fitted cubic splines through the data points, using the interactive fitting task CURFIT in IRAF. Individual data points from the rotation curves were weighted according to their errors (see below); points that were clearly offset from the main rotation curve were eliminated during the fits. The resulting curves are smooth but still follow the general behaviour that underlies the individual data points; they will

be used in the remainder of the paper to study the shapes of the rotation curves and possible correlations with global properties of the galaxies (section 6). They are plotted as bold lines in the rotation curve panels in appendix C.

Finally, a few basic quantities are derived from the rotation curves. The rotation curves were classified on the basis of the quality and reliability of the data. Galaxies which are symmetric, show no signs of strong non-circular motion and have well-defined orientation angles are classed as category I. This class contains the following galaxies: UGC 2953, 3205, 4605, 6786, 6787, 8699, 9133 and 12043. Category II contains galaxies with, for example, mild asymmetries, bar-induced streaming motions or signs of interactions or tidal distortions, as well as galaxies for which the orientation angles could not be constrained as accurately. The following galaxies were classed as category II: UGC 2487 (Seyfert nucleus), 2916 (interacting, lopsided), 3546 (strong bar and Seyfert nucleus), 3580 (lopsided), 3993 (inclination angle uncertain), 4458 (possibly tidally disturbed), 5253 (tidally disturbed), 11670 (large bar), 11852 (bar, kinematically disturbed) and 11914 (inclination angle uncertain). UGC 624 was classified as category III, because of the large-scale asymmetries present in the optical spectrum and particularly in the HI velocity field. The rotation curve of this galaxy is of insufficient quality to be used for mass modelling. The classification of the rotation curves is listed in column (11) of table 2.

We determined by eye the maximum and asymptotic rotation velocities, $V_{\rm max}$ and $V_{\rm asymp}$ respectively. They are listed in table 2 and indicated with the horizontal arrows in the bottom right panels of the figures in appendix C. Similarly, the rotation velocity at 2.2 R-band disk scale lengths, $V_{\rm 2.2h}$ was determined.

From the velocity at the outermost point of the rotation curve, the total enclosed mass is calculated as:

$$M_{\rm enc} = \frac{V_{\rm out}^2 R_{\rm out}}{G} = 2.325 \cdot 10^5 \left(\frac{V_{\rm out}}{\rm km/s}\right)^2 \frac{R_{\rm out}}{\rm kpc}\,{\rm M}_\odot, \qquad (1)$$

with $V_{\rm out}$ the velocity at the last measured point and $R_{\rm out}$ the corresponding radius. The resulting masses are listed in table 2 as well. In this calculation, it was implicitly assumed that the mass distribution interior to $R_{\rm out}$ is spherical. If a significant fraction of the total mass is concentrated in a flat distribution, the value derived here is an upper limit.

3.4 Rotation curve errors

Many factors can cause errors in the derived rotation velocities, both statistical and systematic. For a meaningful interpretation of the results, it is crucial to make a reliable estimate of all relevant uncertainties and much effort was therefore put into the identification and quantification of possible sources of errors.

We account for three main contributions to the errors in the rotation curves. The first is simply the measurement error ΔV_m. For the HI data, this is given by the ROTCUR algorithm, based on the dispersion around the fitted tilted ring velocities; for the optical data, it is the fitted error on the profile centre, given by the Gaussian fitting routine. For the manually adapted velocities, the measurement errors were estimated by eye, based on the shape of the line profiles and the degree to which the data are degraded by beam smearing and line-of-sight integration effects. The contribution ΔV_m is usually significant only in the optical rotation curves and in the inner parts of the HI rotation curve, where only few points are available on the velocity field. At larger radii in the HI rotation curves, where each tilted ring covers many data points in the velocity field, the measurement error is usually small ($\sim 1-2\%$).

The second contribution ΔV_{nc} comes from kinematical asymmetries and non-circular motions in the galaxies. These were estimated by deriving rotation curves for the approaching and receding sides of the galaxies separately. Additional tilted ring models were fitted to the approaching and receding sides of the velocity fields and the resulting rotation curves were combined with the fitted velocities from the corresponding parts of the optical spectra. The resulting rotation curves are shown with the crosses and plus-signs respectively in the bottom right panels in the figures in appendix C. The error in the rotation curve ΔV_{nc} was then estimated as one fourth of the difference between the rotation velocities measured for each side separately (cf. Swaters 1999). With this, rather ad hoc, assumption, the difference between the rotation velocity for each side separately and the average value represents a 2σ deviation. Note that small-scale non-circular motions, or asymmetries perpendicular to the major-axis, are not accounted for in this estimate.

The first two contributions to the rotation curve errors, ΔV_m and ΔV_{nc} were added quadratically, and are shown with the errorbars in the figures in appendix C.

The third contribution to the rotation curve errors comes from the uncertainty in the orientation of the gas disks. The main contribution comes from the uncertainty Δi in the inclination angle, estimated as in section 3.1. Errors in position angle are usually much smaller, and moreover, only contribute in second order to the rotation curve errors; in practice, they can be neglected compared to the uncertainties in inclination. The effect of the inclination errors on the rotation curves is derived as follows. The rotation velocities $V_{\rm rot}$ in the rotation curve can be written as $V_{\rm rot} \propto V_{\rm rad}/\sin i$, where $V_{\rm rad}$ is the measured radial velocity from either the optical spectrum or the HI velocity field. Thus, an error Δi in the inclination leads to an error ΔV_i in the rotation velocity of

$$\Delta V_i = \frac{V_{\rm rot}}{\tan i}\,\Delta i_{\rm rad}, \qquad (2)$$

where $\Delta i_{\rm rad}$ is measured in radians. So, not only is it more difficult to derive the inclination accurately for near face-on galaxies, the resulting uncertainty in the rotation velocities due to a given error Δi becomes progressively larger as well.

The derived errors $\Delta V_i(r)$ are indicated with the shaded regions in the bottom right panels in the figures in appendix C; for clarity, they are drawn around the smoothed rotation curves, rather than around the individual data points. Note that these errors account not only for systematic *offsets* of the rotation curves (due to a global misfit of the inclination), but also for the effect of undetected or misfitted warps, which would alter the *shape* of the rotation curves.

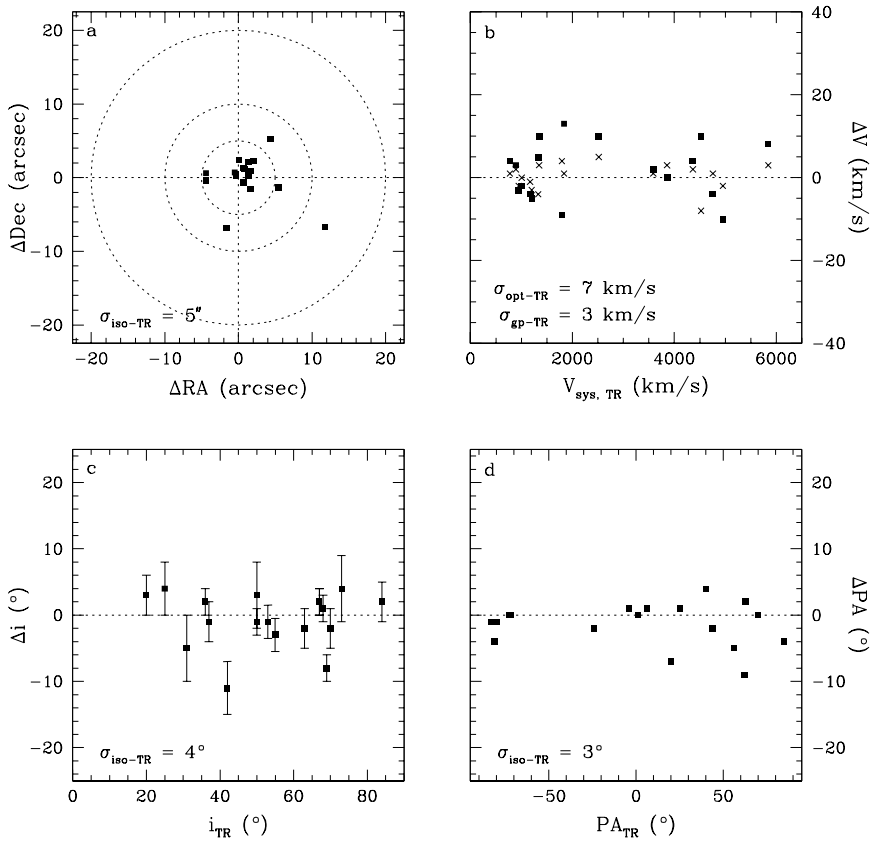

Figure 2. Comparison of global tilted ring (TR) parameters with values from other sources. Data points give offsets of central position (a), systemic velocity (b), inclination (c) and position angle (d) with respect to the values derived from the tilted ring analysis. For warped galaxies, the tilted ring values in the inner regions were used, such that they correspond to the same regions as probed by the optical observations. Filled squares represent the values from the optical isophotal analysis from Paper II (a, c, d) or from the optical spectra (b). The crosses in panel b show the comparison with the systemic velocities derived from the global HI profiles (Paper I). The errorbars in panel c show the adopted uncertainties in the tilted ring inclinations. The standard deviations of the distributions are given in the bottom left corner of each panel. Cases where parameters from different sources were not independently derived (e.g. UGC 624) are not considered here.

4 PARAMETER COMPARISON

A proper derivation of a rotation curve depends crucially on the assumed orientation parameters and systemic velocity of the galaxy. It is instructive to compare the values which we assumed for the rotation curves here, derived from the tilted ring fits, with those obtained from other sources.

Figure 2 shows that, in general, there is good agreement between the parameters from the tilted ring analysis and those derived from e.g. the optical isophotal analysis. In most cases, the dynamical and the isophotal centres coincide within a few arcseconds, well within one HI beam. Larger offsets are only observed in galaxies with strong dust features in the optical image (e.g. UGC 3580) or in highly inclined systems (e.g. UGC 8699), where extinction and line-of-sight integration effects complicate a proper determination of the central position. The observed offsets can be fully explained by observational effects, and no galaxies seem to have a true, physical offset between the dynamical and morphological centres.

A comparison of the systemic velocities from different methods shows that they all agree within 5 – 10 km/s. In galaxies with well-resolved HI velocity fields, however, the tilted ring systemic velocity is the preferred value, as it uses dynamical information from the entire gas disk. The other methods are expected to have larger intrinsic errors, so the dispersions given in the figure will probably come predominantly from errors in those measurements; the typical error with which one can determine the systemic velocity using tilted ring models is probably of the order of 2 – 4 km/s.

The disk orientation parameters derived from the optical isophotes usually agree within a few degrees with the tilted ring parameters. In particular, panel (c) shows that our assumed errors Δi on the inclinations are reasonable. Only 2 galaxies show an offset between the isophotal and kinematical inclination angles that is significantly larger than the assumed error. One is UGC 2916, which is interacting with a companion galaxy. Close inspection of the fitted optical ellipticities (Paper II) shows that the shape of the isophotes at intermediate radii is consistent with the kinematical inclination; the outer isophotes are most likely disturbed by the tidal influence of the companion. The other case is UGC 6787, where the isophotal inclination is poorly constrained due to the influence of the dominant bulge. Again, since the tilted ring analysis uses dynamical information from the entire gas disks, it will generally give more accurate values for the inclination and position angles, so figure 2 mostly shows the uncertainties in the isophotal pa-

rameters. Note that the inclinations from LEDA have a large scatter around our values, with discrepancies up to 20°.

5 WARPS

It has been known for a long time that the outer parts of the gas disks of many spiral galaxies are not coplanar with the inner disk, but that they are 'warped' (Rogstad et al. 1974; Sancisi 1976). Bosma (1991) reported that at least 50% of all galaxies are warped. More recently, García-Ruiz et al. (2002) studied 26 edge-on galaxies and found that *all* galaxies with an HI disk more extended than the stellar one are warped.

Most galaxies in our sample are fairly face-on and warps are therefore seen less easily than in Garcia-Ruiz' galaxies. Nevertheless, we can infer the presence of warps from the tilted ring fits to the velocity fields. Inspection of the figures in appendix C shows that the fitted inclination or position angles show significant radial variations in 14 of our 19 galaxies. For three of the remaining five galaxies (UGC 624, 3993 and 8699), the quality of the velocity fields is insufficient to put strong constraints on the orientation of the gas disks and we cannot exclude the possibility that these systems are warped as well. Only two galaxies, UGC 3205 and 3546, show little variation in the fitted orientation angles (the variations in the inner part of UGC 3205 can be attributed to bar-induced streaming motions) and seem to have no detectable warp at all.

Briggs (1990) claimed that warping tends to set in in the outer parts of the optical disk (around R_{25}). Although many of the galaxies in our sample are consistent with having a flat gas disk within the optical radius, we also find a few counter-examples. The velocity fields of UGC 6786, 6787 and 11852 show clear signs of warping in the inner parts. The first two systems are unbarred and the observed variations in their orientation parameters must be real. UGC 11852 has a bar, but it is smaller than the HI beam; the observed warping occurs at larger radii and must, again, be real. Note, however, that in all three cases, the inner warps are mild. Strong warps are only observed outside the bright optical disks, e.g. in UGC 9133 and 11852.

6 ROTATION CURVE SHAPE

The shape and amplitude of a galaxy's rotation curve are directly related to the gravitational field in the midplane of its disk, and thus to the mass distribution of its main components. A systematic study of the shapes of rotation curves, and a comparison with the optical properties of the galaxies, can therefore yield important information on the distribution and relative importance of dark matter in galaxies. In particular, many studies have addressed the correlation between the distribution of luminous matter and the shape of a rotation curve (see the introduction for references). If the luminous matter plays a significant rôle in the dynamics of galaxies, the shape of a rotation curve must depend on the distribution of the luminous matter. On the other hand, if dark matter is dominant, such a correlation will be much weaker or completely absent.

In figure 3, we show a compilation of all the rotation curves in our sample. In the left hand panels, the rotation curves are plotted on the same physical scale; in the right hand panels, all radii are scaled with the R-band scale lengths of the stellar disks (from Paper II). Although there is a large variety in rotation curve shape among the galaxies in our sample, there are also some general features which can be recognised from this figure and from the individual rotation curves shown in appendix C.

Almost all rotation curves in our sample rise extremely steeply in the central regions. In only one case (UGC 12043 (#19)) do we see the 'standard' gradual solid-body-like rise of the rotation curve, before flattening out at about 3 disk scale lengths. In all other cases, the initial rise of the rotation curve is unresolved, even in the optical spectrum, and the rotation velocities rise from 0 to $\gtrsim$ 200 km/s within a few hundred parsecs (or, similarly, within a fraction of a disk scale length). In some cases (such as UGC 2953 (#4), 3205 (#5) or 3580 (#7)), the steep central rise is followed by a more gentle increase before the maximum rotation velocity is reached; in other cases (e.g. UGC 4458 (#9), 5253 (#11), 9133 (#15)), the rotation curve rises to its maximum immediately.

At larger radii, many rotation curves show a marked decline. In several cases (for example UGC 2487 (#2), 2916 (#3), 5253 (#11)), the rotation curves are more or less flat in the inner regions and the decline sets in quite suddenly around the edge of the optical disks (near R_{25}); this behaviour is similar to that in e.g. NGC 3992 (Bottema & Verheijen 2002) and NGC 5055 (Battaglia et al. 2006). But there are also cases where the rotation velocities start decreasing well inside the optical disk (e.g. UGC 2953 (#4), 9133 (#15)), or even right from the first point in the rotation curve (UGC 4458 (#9)).

Although the total decline in the rotation curve can be large (more than 50% in the case of UGC 4458 (#9); $\sim$ 25% for UGC 9133 (#15) and 11852 (#17)), all declining rotation curves appear to flatten out at large radii. No rotation curves are found with a fully Keplerian decline in the outer regions, indicating that we have not yet reached the point where the mass density becomes negligible. Thus, although the rotation curves of massive, early-type disk galaxies look remarkably different from those of later-type spiral galaxies at small and intermediate radii (with the latter generally lacking the steep rise in the centre and the decline at intermediate radii; Corradi & Capaccioli 1990, Spekkens et al. 2005, Catinella et al. 2006), they show the same 'flatness' in the outer regions, proving that they too must contain large quantities of dark matter. An interesting possible exception is UGC 4458, whose rotation curve only flattens out in the very outer regions. Given the large uncertainties in the outer data points due to the face-on orientation, we cannot strictly rule out that this rotation curve keeps declining in Keplerian fashion. We will investigate this issue, and its implications for the dark matter content in this galaxy, in more detail in our subsequent paper on the mass modelling.

It is worth mentioning that many galaxies show distinct features in their rotation curves (e.g. UGC 6787 (#13), 8699 (#14); see also the notes on individual cases in appendix A). Only few galaxies have smooth rotation curves without 'bumps' or 'wiggles' and the declines at intermediate radii are rarely featureless and monotonous. Although these irregularities may sometimes be caused by e.g. noise

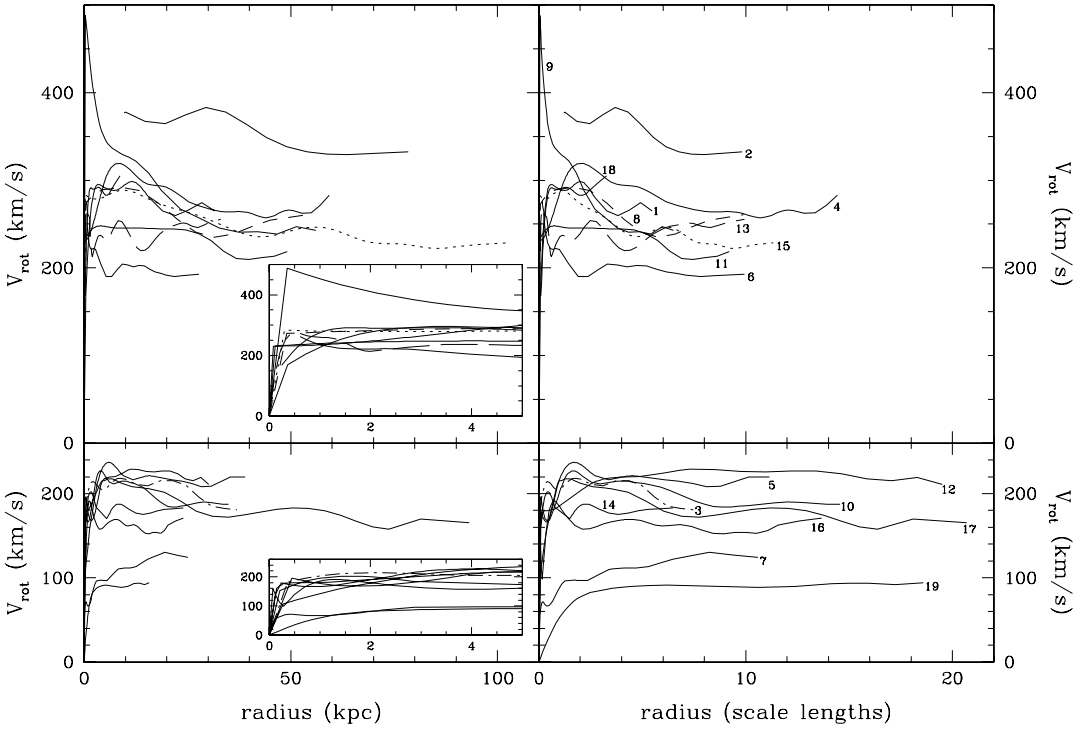

Figure 3. Compilation of rotation curves from all galaxies in the sample. The top panels show the rotation curves with $V_{\rm max} > 250\,$km/s, the bottom panels show those with $V_{\rm max} < 250\,$km/s. In the left hand panels, the rotation curves are plotted on the same physical scale; the insets show the inner 5 kpc of all curves. In the right hand panels, all radii are scaled with the R-band disk scale lengths. The curves are identified with the sample numbers from table 1. To limit confusion, a few curves are plotted using different linestyles: UGC 2916 (#3, dot-dash), 3993 (#8, short dash), 6787 (#13, long dash) and 9133 (#15, dots).

or non-circular motions of the gas, they can often be recognized on both sides of the optical spectra or HI velocity fields and must, in most cases, reflect small-scale features in the underlying mass distribution. In particular, we will show in our forthcoming publication on the mass models that the 'wiggles' and the detailed shape of the drop-off in the rotation curves can, in some cases, be linked to features in the light or gas distributions and can be used to constrain the relative contributions of the luminous and dark matter in these galaxies.

In some cases, such as UGC 2953 (#4), 3993 (#8) or 11670 (#16), there are indications that the rotation curves start to rise again at the outer edges of the HI disks. Whether this effect is real or an artefact in the data is hard to tell. The corresponding points in the HI velocity fields were derived from low signal-to-noise ratio line profiles and have large uncertainties. Furthermore, we cannot exclude the possibility that the gas in the outer regions moves on non-circular orbits, or that we have not determined the inclination of the orbits correctly. Follow-up observations at higher sensitivity are required to investigate this in more detail.

6.1 Correlations with optical properties

To investigate the dependence of rotation curve shape on the optical properties of the galaxies, we have ordered the rotation curves from our sample according to several parameters. In figures 4 and 5, we present a compilation of our rotation curves in a similar fashion as Casertano & van Gorkom (1991); the rotation curves are ordered according to the maximum rotation velocity $V_{\rm max}$ and the R-band disk scale length (figure 4) or bulge-to-disk luminosity ratio (figure 5). In figure 6, we have divided our galaxies into different subsamples, according to several optical parameters, and plot the rotation curves for each subsample separately.

6.1.1 inner rotation curves

Early results by Rubin et al. (1985) showed that the inner shape of a rotation curve is coupled to a galaxy's luminosity: bright galaxies have steeply rising rotation curves, whereas low-luminosity systems reach the maximum rotation velocity at relatively larger radii. This relation was later confirmed by several other studies (e.g. Broeils 1992; Persic et al. 1996; Verheijen 1997; Swaters 1999). The galaxies with the lowest luminosity (and corresponding maximum velocity) in our sample (UGC 3580 (#7) and 12043 (#19)) follow this trend and have rotation curves which rise relatively slowly. In particular, UGC 12043 (#19) is the only galaxy in our sample which completely lacks the characteristic steep rise in the centre; instead, its rotation velocities increase gradually, in solid-body fashion and only reach the maximum around 3 disk scale lengths. The remaining galaxies in our sample, however, seem to indicate that the systematic progression breaks down above a maximum rotation velocity of $\sim$200 km/s (see figure 4). All galaxies with a rotation velocity larger than $\sim$200 km/s have the characteristic steep rotation curve in the centre. Whether the rotation velocities continue to increase after this initial rise,

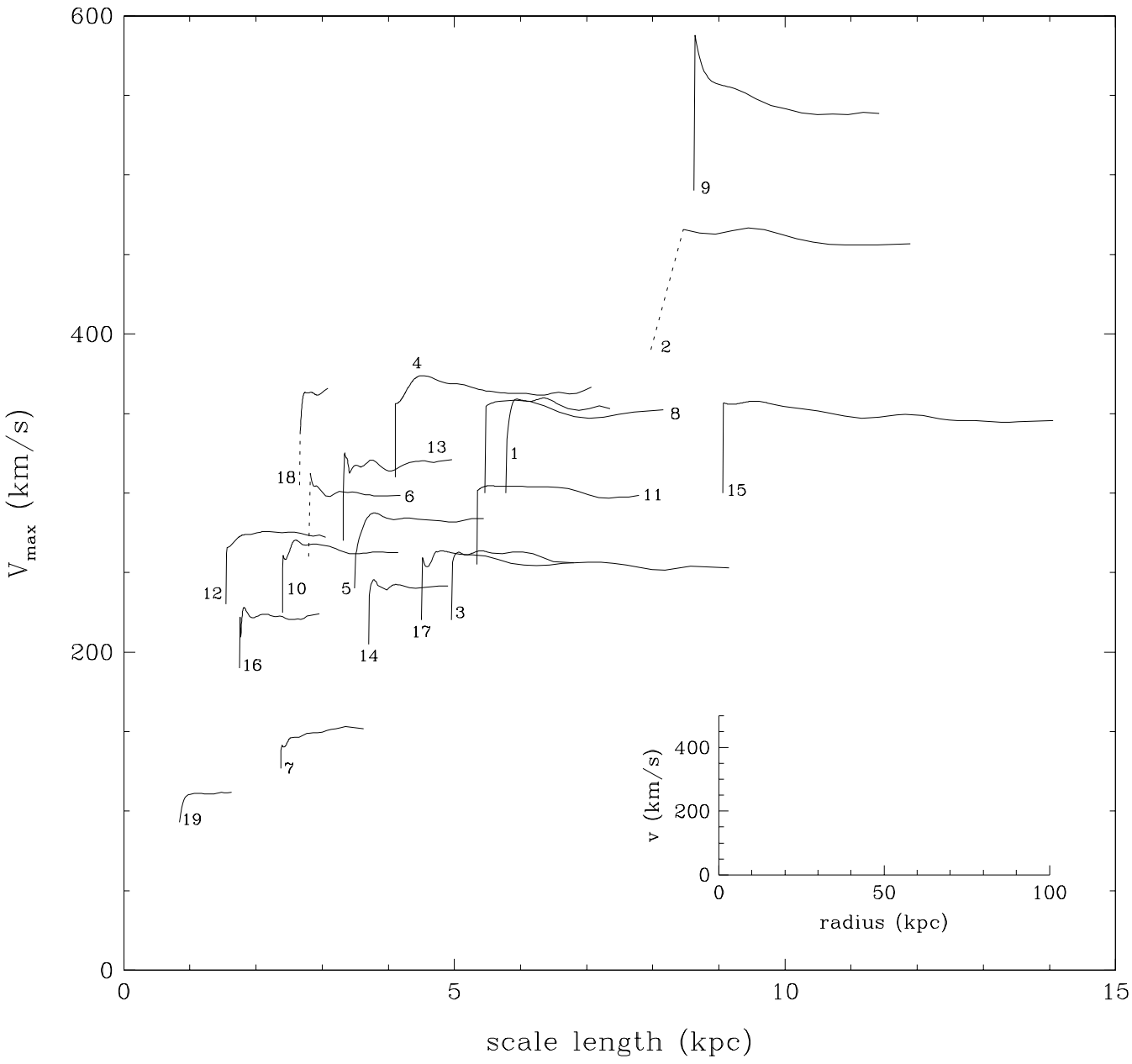

Figure 4. Compilation of rotation curves following Casertano & van Gorkom (1991). The origin of each rotation curve is placed according to the maximum rotation velocity $V_{\rm max}$ and the R-band exponential scale length of the stellar disk. Dashed lines are used to indicate the origins for galaxies where the central rotation curve was not measured. The individual rotation curves are labelled using the sample numbers from table 1 and scaled in radius and velocity, as indicated with the small axes at the bottom right. The scale lengths for UGC 4605 and 6786 (#10 and #12) are estimates only, so their exact position in the figure is uncertain.

or whether the maximum is reached in the very centre, does not seem to depend on the total luminosity of the galaxy.

Instead, the shape of the rotation curve in the inner regions seems to depend more strongly on the concentration of the stellar light distribution. This can be seen most clearly in figure 5 and in the bottom panels of figure 6, where the rotation curves are ordered according to the bulge-to-disk luminosity ratio and the more generic measure of light concentration R_{80}/R_{20} respectively. These figures show that the rotation curves of galaxies with faint bulges and a relatively diffuse stellar light distribution continue to rise after the steep central part, and reach the maximum outside the bulge-dominated regions (e.g. UGC 2953 (#4) and 3205 (#5)). On the other hand, the rotation curves of galaxies with highly concentrated light distributions rise to the maximum immediately. This also explains why UGC 12043 (#19) has such a shallow central rotation curve: it has no bulge component at all. The only system with a small bulge which appears to reach its maximum rotation velocity at very small radii is UGC 3546 (#6), but this galaxy has a Seyfert nucleus which makes its central rotation velocities highly uncertain (see the errorbars in the figure in appendix C); it is well possible that the rotation curve of this galaxy rises more slowly than we have derived here.

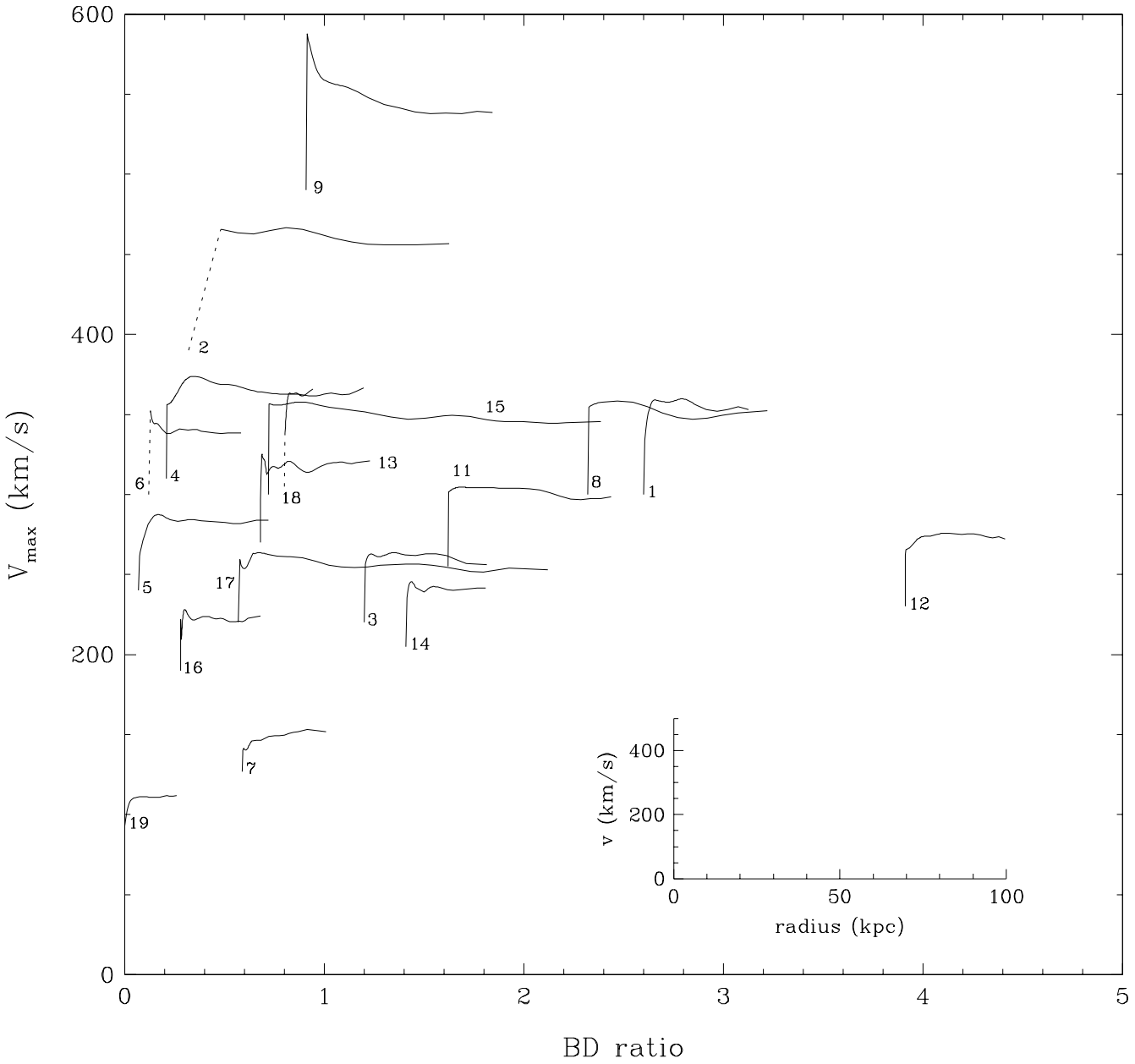

Figure 5. Compilation of rotation curves similar to figure 4, this time with the origin of each curve placed according to the maximum rotation velocity $V_{\rm max}$ and the R-band bulge-to-disk luminosity ratio. UGC 4605 was not included in this figure, since no bulge-disk decomposition was available for this galaxy.

Thus, our data appear at odds with the claim of Rubin et al. (1985) and Burstein & Rubin (1985) that optical morphology does not influence the shape of a rotation curve and that large amounts of dark matter must be present at all radii. Our data indicate that at least the bulge stars have a strong influence on the central rotation curves, and suggest that they dominate the gravitational potential in the inner regions (in agreement with Corradi & Capaccioli 1990, Verheijen 1997 and Sancisi 2004).

6.1.2 outer rotation curves

Inspection of figures 4 – 6 shows that the shape of the rotation curves in the outer parts is correlated with the luminosity of the galaxies: luminous galaxies are more likely to have a declining rotation curve than low-luminosity systems (in agreement with Casertano & van Gorkom 1991 and Broeils 1992). This is shown in a more quantitative way in panel a) of figure 7, where we plot the ratio of asymptotic and maximum rotation velocity as a function of total absolute magnitude. This figure shows that *all* early-type disk galaxies with $M_R < -20$ have at least a modest decline in their rotation curve.

The strength of the decline shows, however, little dependence on the *shape* of the light distribution. Casertano & van Gorkom (1991) concluded that, in a sample of galaxies of type Sb and later, the most strongly declining rotation curves occur in systems with a compact light

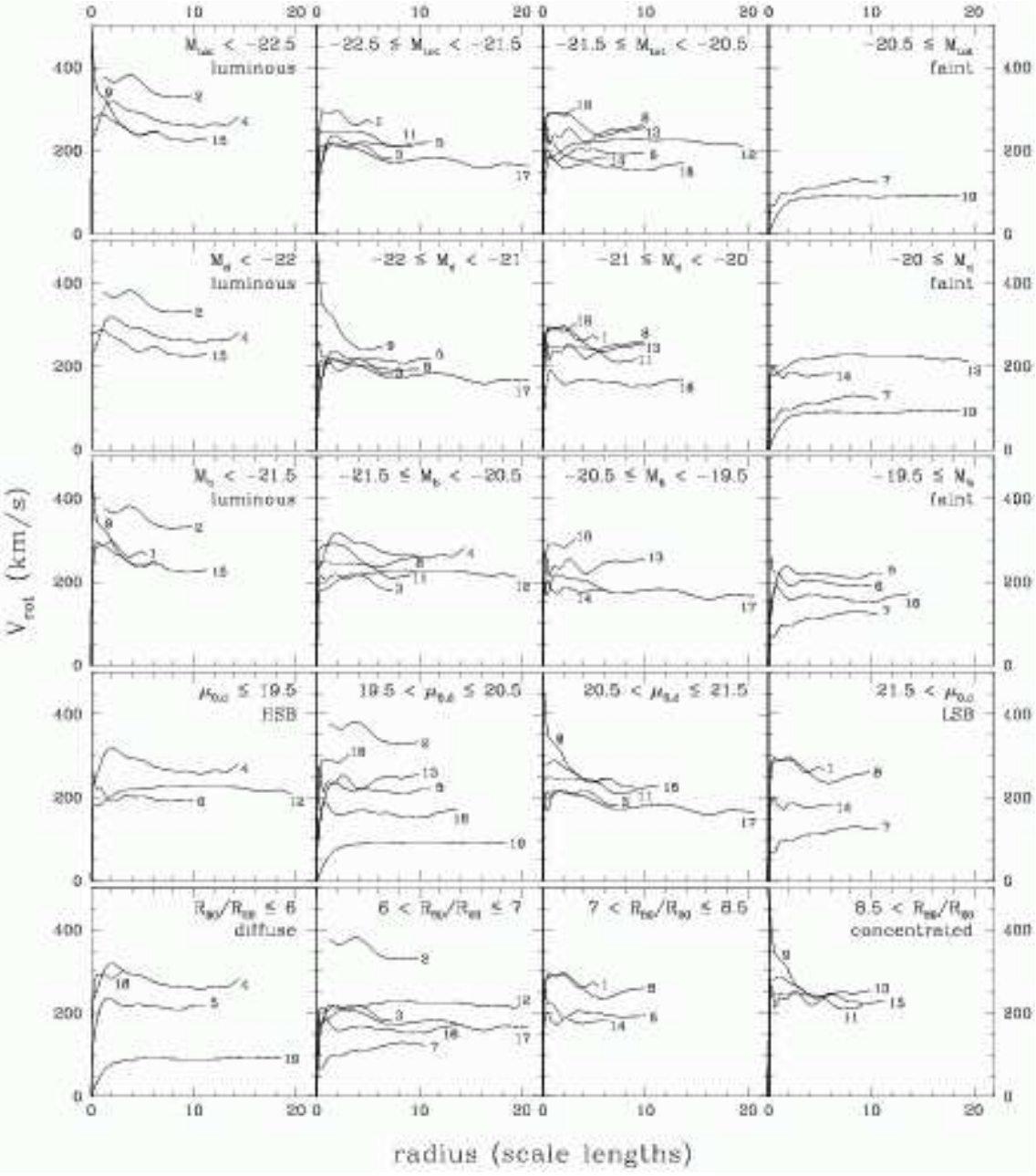

Figure 6. Rotation curves ordered according to (from top to bottom) absolute magnitude of the entire galaxy, absolute magnitude of the stellar disk, absolute magnitude of the stellar bulge, central surface brightness of the stellar disk and compactness of the stellar light distribution (measured by the ratio of the effective radii R_{80} and R_{20} which contain respectively 80 and 20% of the light). All parameters are derived from the R-band images (see tables A3 and A4 in Paper II). The bins are chosen in order to distribute the rotation curves evenly over the panels. All rotation curves are labelled with the sample numbers from table 1 and scaled with the R-band disk scale lengths. Since no accurate photometry is available for UGC 4605 (#10), this galaxy is not included in these plots. Furthermore, UGC 12043 (#19) does not have a bulge component and is not included in any of the plots in the third row.

distribution, where 'compact' in their terminology meant 'small disk scale length'. Our data show that such a correlation does not exist for early-type disks, as our sample also contains a number of galaxies with large scale lengths which have falling rotation curves (see figure 4). This is in agreement with Broeils (1992), who also found a number of large galaxies with declining rotation curves. In fact, two of the galaxies in our sample with the most strongly declining rotation curves (UGC 4458 (#9) and 9133 (#15)), have large scale lengths (8.6 and 9.1 kpc respectively). Panel b) in figure 7 shows that, if a trend with linear size of the galaxies exists at all, it is in the opposite direction as observed by Casertano & van Gorkom (1991): larger galaxies have on average more strongly declining rotation curves.

No trend is seen when, instead of the disk scale length, we use the more generic parameter R_{80}/R_{20} to define the compactness of the stellar light distribution (bottom panels in figure 6 and panel c) in figure 7). Declining rotation

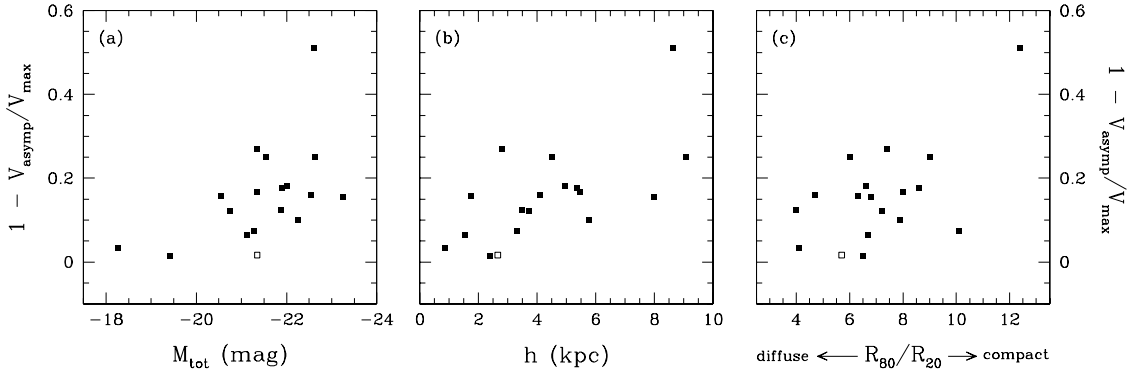

Figure 7. Strength of the decline in the rotation curves vs. total magnitude (a), scale length of the stellar disk (b) and ratio of the effective radii R_{80} and R_{20} (c) (all measured from the R-band images). The open symbol indicates UGC 11914; due to the small radius of the last measured point in the rotation curve, its asymptotic rotation velocity is poorly defined (see also appendix A). Since no accurate photometry is available for UGC 4605, this galaxy is not included in these plots.

curves are seen both in galaxies with a compact light distribution and in galaxies with a more diffuse stellar component (such as UGC 2487 (#2) or 2953 (#4)). Note, however, that according to this criterion, the galaxy with the strongest decline in its rotation curve is also the most concentrated: UGC 4458 (#9).

6.2 The Universal Rotation Curve for early-type disk galaxies

Persic et al. (1996) claimed, based on a study of over 600 optical rotation curves and a small number of HI rotation curves, that the shape of a rotation curve is solely governed by the galaxy's luminosity and can be described by the following simple formula:

$$V_{\rm URC}(x) = V_{\rm opt}\left\{(0.72+0.44\log\lambda)\frac{1.97x^{1.22}}{(x^2+0.78^2)^{1.43}} + 1.6\,e^{-0.4\lambda}\frac{x^2}{x^2+1.5^2\lambda^{0.4}}\right\}^{1/2}. \quad (3)$$

Here, $x = R/R_{\rm opt}$ is the radius expressed in units of the optical radius $R_{\rm opt}$, the radius encompassing 83% of the light. $V_{\rm opt}$ is the rotation velocity at $R_{\rm opt}$ and $\lambda = L_B/L_B^*$ is the B-band luminosity of the galaxy scaled with L^*. In principle, $V_{\rm opt}$ can also be related to the luminosity via the Tully-Fisher relation, but since we are mostly interested in the *shape* of the rotation curve here, we empirically determine $V_{\rm opt}$ from our observed rotation curves.

This Universal Rotation Curve (URC) has received considerable attention in the literature, as it implies (together with other scaling relations such as the Tully-Fisher relation) a tight connection between the luminous and dark matter in galaxies and, as such, has important consequences for the theory of galaxy formation (Dalcanton et al. 1997; Hernandez & Gilmore 1998; Elizondo et al. 1999). However, from the observational point of view, no consensus has yet been reached concerning the general applicability of the concept of the URC to real galaxies. Although the URC seems to give a reasonable description of the general trends in rotation curve shapes, it was readily noted that individual rotation curves often show large deviations from the URC (Courteau 1997; Verheijen 1997; Willick 1999; Garrido et al. 2004) and that other parameters than luminosity must also influence a galaxy's rotation curve (e.g. surface density, bulge-to-disk ratios, etc., see also Roscoe 1999). Our findings that the rotation curves of early-type disk galaxies have distinctly different shapes (steep central rise, decline at intermediate radii) than those of later-type systems of similar luminosity, and that within our sample, the rotation curve shape is only weakly coupled to luminosity and rather depends on factors such as light concentration, bulge-disk ratio, etc., raise additional questions on the ability of the URC to describe rotation curves of all classes of disk galaxies.

In figure 8, we compare the predicted rotation curves from equation 3 to our observed rotation curves. We did not measure the optical radius $R_{\rm opt}$ for our galaxies, but use R_{80}, the radius containing 80% of the light in the B-band (see table A3 in Paper II), as an approximation instead. All velocities are scaled with V_{80}, the rotation velocity at R_{80}. UGC 4605 was omitted from the analysis, since no accurate photometric data were available. The most obvious result from figure 8 is that the URC completely fails to account for the steep central rise in our rotation curves. In all galaxies, except the bulgeless system UGC 12043, the URC severely under-predicts the rotation velocities in the centre. For UGC 2953, it is hard to see the discrepancy in the figure due to the crowding of the points, but also in this case, the observed velocities inside $0.4\,R_{80}$ lie far above the predicted curve. This failure in the inner regions is, however, not surprising, as Persic et al. (1996) derived their relations specifically for disk-dominated galaxies and did not take bulges into account.

In the outer parts, the agreement is good in some cases (e.g. UGC 2953, 3205, 9133), but there are also many galaxies where the observed rotation curves have a markedly different shape than the predictions from the URC. In particular, the slope of the outer rotation curve seems to be poorly predicted by the URC, with the observed rotation curves flat instead of rising (e.g. UGC 6786, 11670, 12043), declining instead of flat (UGC 11852) or not declining rapidly enough (UGC 2487). But some of these differences at larger radii may be related to the presence of the bulges as well. Not only do bulges influence the observed rotation velocities in the galaxies, they also change the shape of the predicted rotation curve by altering the total luminosity and the opti-

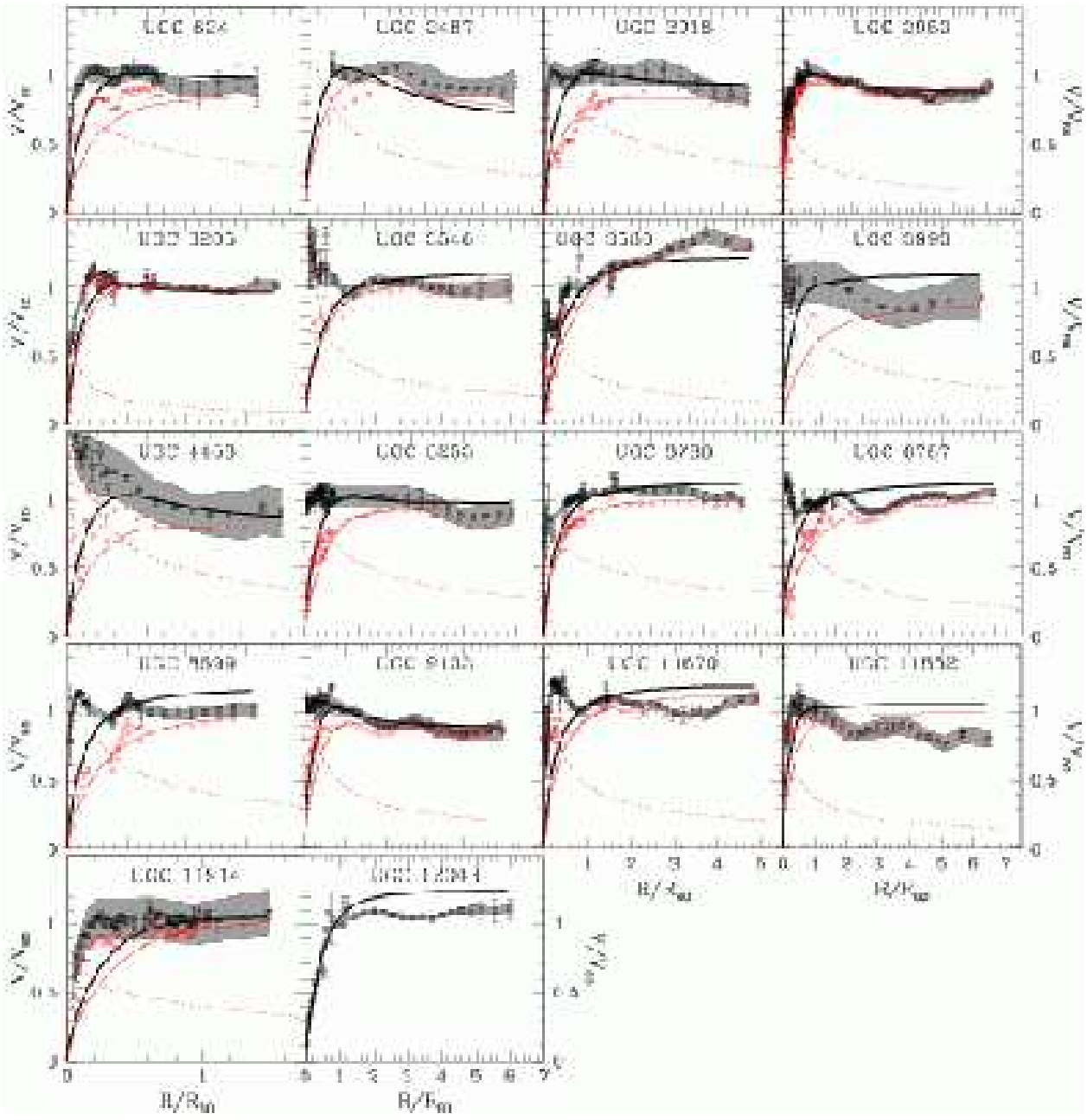

Figure 8. Comparison of our rotation curves (black data points with error bars) with the Universal Rotation Curve from Persic et al. (1996) (bold black lines). Shaded regions give the uncertainties due to inclination errors. Red data points show the rotation curves after subtraction of the bulge component (shown with the dashed red lines; not for the bulgeless galaxy UGC 12043). The solid red line shows the URC for the disk component. All rotation curves are scaled with R_{80}, the radius containing 80% of the total B-band light (from Paper II) and V_{80}, the rotation velocity at R_{80}. See text for details.

cal radius; thus, they may cause discrepancies over the full length of the rotation curves.

To investigate to what extent the difference between the observed rotation curves and the URC can be explained by the presence of the massive bulges in our galaxies, we have subtracted their contribution from the observed and predicted rotation curves; the results are shown in red in figure 8. The bulge contributions were taken from our mass models, which will be presented in a forthcoming publication. The solid red lines show the predicted rotation curves from equation 3, now using the absolute B-band magnitudes of the disk components (taken from Paper II).

The correction for the bulge influence has indeed alleviated some of the discrepancies, especially in the central parts; some galaxies show almost perfect agreement with the predicted rotation curves now (e.g. UGC 2953, 6786, 9133). However, even after the bulge corrections, many differences remain. Most rotation curves still rise more rapidly than predicted by the URC and reach a flat plateau where the URC is still rising (e.g. UGC 624, 3205, 3546, 3993, 4458, 11670, 11852). Also in the outer regions, the observed slopes

of the rotation curves often still differ from the predicted ones, although the differences are generally smaller than in the original curves.

In conclusion, the foregoing analysis confirms the dependence of rotation curve shape on morphological type, with bulge-dominated, early-type disk galaxies having distinctly different rotation curves than late-type spirals of similar luminosity. Thus, a universal rotation curve that depends only on luminosity is inadequate to account for the observed diversity in rotation curve shapes along the Hubble-sequence. Although the URC of Persic et al. (1996) may have its virtue as an empirical tool to parameterise global trends of several properties of *disk-dominated* galaxies (surface brightness, size, etc.) with luminosity and the reflection of those on the gravitational fields, additional parameters are required to account for the presence of bulges in earlier-type disks. In addition to the deviations in the inner regions, we have shown that the detailed shape of the drop-off in the outer parts of our rotation curves is not well reproduced either. Clearly, real galaxies are more complex than the simple URC prescription suggests and other factors than luminosity must contribute to the detailed shape of a rotation curve as well.

7 DISCUSSION AND CONCLUSIONS

In this paper, we have derived rotation curves for a sample of 19 early-type disk galaxies ($S0^-$ – Sab) spanning almost 2 decades in optical luminosity. The majority of the galaxies are luminous, with $M_B < -20$. The rotation curves were derived from a combination of HI synthesis observations and long-slit optical spectroscopy of the ionised gas and probe the rotational velocities and mass distributions on scales ranging from 100 pc to 100 kpc. Almost all of the rotation curves share a number of properties, which appear to be typical for this type of galaxies.

The rotation velocities generally rise rapidly and often reach values of 200 – 300 km/s (and up to 500 km/s for extreme cases such as UGC 4458) within a few hundred parsecs from the centres of the galaxies. After the initial steep rise, the rotation curves show a diversity in shapes. In some cases, the rotation velocities gradually increase further and reach the maximum at intermediate radii. In other cases, the rotation curves remain flat after the initial rise, or even start to decline immediately. This diversity in shape appears to be related to differences in the light distribution in these galaxies: galaxies with concentrated light distributions and luminous bulges generally reach the maximum rotation velocity at small radii, whereas galaxies with a more diffuse stellar component, or small bulges, generally have rotation curves which peak further out.

At larger radii, most rotation curves decline, with the asymptotic rotation velocity typically 10 – 20% lower than the maximum. The strength of the decline is coupled to the luminosity of the galaxy, more luminous galaxies having on average more strongly declining rotation curves, in agreement with Casertano & van Gorkom (1991). However, we cannot confirm another claim of Casertano & van Gorkom, that declining rotation curves occur preferentially in galaxies with a compact light distribution. By 'compact', these authors meant 'small disk scale length'. In agreement with Broeils (1992), our sample also contains a number of galaxies with large scale lengths which have falling rotation curves. Interestingly, two recent studies (Spekkens et al. 2005; Catinella et al. 2006) showed that later-type galaxies, even those with high optical luminosity, do *in general* not have declining rotation curves. In contrast, we find that declining rotation curves are a *characteristic feature* of massive, *early-type* disk galaxies. This seems to suggest that, although Casertano & van Gorkom were correct to claim that the shape of the light distribution determines whether or not a galaxy has a declining rotation curve, the term 'compactness' must be interpreted as the presence of a light concentration (i.e. a bulge) in the centre, rather than a small scale in absolute terms. Note that the two galaxies in Casertano & van Gorkom with the most strongly declining rotation curves (NGC 2683 and NGC 3521) both have a sizable bulge (Kent 1985). Within in our own sample, on the other hand, the strength of the decline in the rotation curves seems barely related to the bulge-to-disk luminosity ratio, or generic light concentration R_{80}/R_{20}. Thus, although our data suggest that the bulge plays an important rôle in this issue, we conclude that it is not possible to extract a single parameter from the light distribution of a galaxy which uniquely determines whether or not it has a declining rotation curve. Rather, it must depend in a more subtle manner on the relative masses, and the details of the mass distributions, of the various luminous and non-luminous components in a galaxy. We will address this issue in more detail in our forthcoming publication on the mass models for our galaxies.

It is important to note that we have not found any rotation curve which declines in Keplerian fashion. In fact, all rotation curves flatten out in the outer regions. Early-type disk galaxies, despite appearing dominated by luminous matter in the central parts, must also contain large amounts of dark matter to explain the shape of the rotation curves in the outer regions.

Two low-luminosity galaxies, UGC 3580 and 12043, have a distinctly different kinematical structure than the other systems in our sample. The rotation curve of the former does rise rapidly in the centre, but where in most other galaxies the rotation velocities decrease or remain constant at large radii, they continue to rise almost all the way till the outer point in the case of UGC 3580 (out to $\sim$8.5 disk scale lengths). UGC 12043 completely lacks the steep central rise in the rotation curve; instead, its rotation velocities increase gradually, in solid-body fashion, before becoming constant outside approximately 3 disk scale lengths. The rotation curves of these two galaxies resemble those of typical late-type and dwarf galaxies which generally have slowly rising rotation curves too (Broeils 1992; Swaters 1999). UGC 3580 and 12043 also have different optical morphologies than most galaxies in our sample (see Paper II) and the conclusion seems justified that low-luminosity early-type disks form an entirely different class of galaxies.

We have compared our rotation curves with the predictions from the Universal Rotation Curve from Persic et al. (1996). Since their model contains only one parameter, the total luminosity, and does not include morphological type, their URC fails to account for the steep central rise in our observed rotation curves. These discrepancies are reduced, but not removed entirely, when we subtract the bulge influ-

ence from the rotation curves. Furthermore, there are also many differences between the observed and predicted rotation curves at larger radii. The concept of a Universal Rotation Curve which depends only on luminosity appears to be insufficient to account for the observed diversity in rotation curve shape; other factors must contribute to the detailed shape of a rotation curve as well.

All in all, the results presented here show that rotation curves form a multi-parameter family. Although luminosity is clearly a major factor determining the shape of a rotation curve, other parameters are important too. In particular, early-type disk galaxies have distinctly different rotation curves than their later-type counterparts, an effect which we have shown is mostly due to the presence of bulges in these systems. This is in contrast with some previous claims (e.g. Rubin et al. 1985; Burstein & Rubin 1985; Persic et al. 1996) that the shape of the rotation curves is determined by a galaxy's luminosity only and that the way the light is distributed has little influence. Our results contradict this and, in fact, indicate that above rotation velocities of about 200 km/s, the total luminosity has little impact on the shape of the central rotation curve and that, instead, the *shape* of the stellar light distribution governs the dynamics in the inner parts. Our findings have important consequences for our understanding of the structure of galaxies. In particular, our data strongly suggest that, at least in the central regions of the early-type galaxies presented in this study, the luminous matter dominates the gravitational potential, with dark matter only starting to play a role outside the bulge-dominated regions. We will investigate this issue in more detail in a forthcoming publication, where we construct detailed mass models for the galaxies in our sample and study the relation between luminous and dark matter in a more quantitative way.

ACKNOWLEDGEMENTS

We would like to thank Benne Holwerda for kindly providing the optical spectra of UGC 2953. We are grateful to Jacqueline van Gorkom and Reynier Peletier for stimulating discussions which helped to improve the early stages of this paper. We would also like to thank the anonymous referee for pointing out several unclarities in the original document, and for helpful suggestions to improve the presentation.

REFERENCES

Atkinson J. W. et al., 2005, MNRAS, 359, 504
Battaglia G., Fraternali F., Oosterloo T., Sancisi R., 2006, A&A, 447, 49
Begeman K., 1987, PhD thesis, Rijksuniversiteit Groningen
Begeman K. G., 1989, A&A, 223, 47
Bertin G., Saglia R. P., Stiavelli M., 1988, ApJ, 330, 78
Bertola F., Cappellari M., Funes J. G., Corsini E. M., Pizzella A., Vega Beltrán J. C., 1998, ApJ, 509, L93
Bosma A., 1978, PhD thesis, Rijksuniversiteit Groningen
Bosma A., 1981, AJ, 86, 1825
Bosma A., 1991, in Warped Disks and Inclined Rings around Galaxies Warped and Flaring HI Disks. p. 181
Bottema R., Verheijen M. A. W., 2002, A&A, 388, 793
Briggs F. H., 1990, ApJ, 352, 15
Broeils A. H., 1992, PhD thesis, Rijksuniversiteit Groningen
Burstein D., Rubin V. C., 1985, ApJ, 297, 423
Côté S., Carignan C., Freeman K. C., 2000, AJ, 120, 3027
Carignan C., Côté S., Freeman K. C., Quinn P. J., 1997, AJ, 113, 1585
Carollo C. M., Stiavelli M., de Zeeuw P. T., Mack J., 1997, AJ, 114, 2366
Carollo C. M., Stiavelli M., Mack J., 1998, AJ, 116, 68
Carollo C. M., Stiavelli M., Seigar M., de Zeeuw P. T., Dejonghe H., 2002, AJ, 123, 159
Carter D., Jenkins C. R., 1993, MNRAS, 263, 1049
Casertano S., van Gorkom J. H., 1991, AJ, 101, 1231
Catinella B., Giovanelli R., Haynes M. P., 2006, ApJ, 640, 751
Corradi R. L. M., Capaccioli M., 1990, A&A, 237, 36
Courteau S., 1997, AJ, 114, 2402
Dalcanton J. J., Spergel D. N., Summers F. J., 1997, ApJ, 482, 659
de Blok W. J. G., McGaugh S. S., van der Hulst J. M., 1996, MNRAS, 283, 18
Edelsohn D. J., Elmegreen B. G., 1997, MNRAS, 287, 947
Elizondo D., Yepes G., Kates R., Müller V., Klypin A., 1999, ApJ, 515, 525
Fathi K., 2004, PhD thesis, Rijksuniversiteit Groningen
Ferrarese L., Ford H. C., 1999, ApJ, 515, 583
Filippenko A. V., Sargent W. L. W., 1985, ApJS, 57, 503
García-Ruiz I., Sancisi R., Kuijken K., 2002, A&A, 394, 769
Garrido O., Marcelin M., Amram P., 2004, MNRAS, 349, 225
Gentile G., Salucci P., Klein U., Vergani D., Kalberla P., 2004, MNRAS, 351, 903
Giovanelli R., Haynes M. P., Rubin V. C., Ford W. K., 1986, ApJ, 301, L7
Giovannini G., Cotton W. D., Feretti L., Lara L., Venturi T., 2001, ApJ, 552, 508
Harms R. J., Ford H. C., Tsvetanov Z. I., Hartig G. F., Dressel L. L., Kriss G. A., Bohlin R., Davidsen A. F., Margon B., Kochhar A. K., 1994, ApJ, 435, L35
Hernandez X., Gilmore G., 1998, MNRAS, 294, 595
Ho L. C., Filippenko A. V., Sargent W. L. W., Peng C. Y., 1997, ApJS, 112, 391
Huchra J. P., Wyatt W. F., Davis M., 1982, AJ, 87, 1628
Hunt L. K., Malkan M. A., 2004, ApJ, 616, 707
Kamphuis J. J., Sijbring D., van Albada T. S., 1996, A&AS, 116, 15
Keel W. C., 1983, ApJ, 268, 632
Kent S. M., 1985, ApJS, 59, 115
Kent S. M., 1988, AJ, 96, 514
Maraston C., Bastian N., Saglia R. P., Kissler-Patig M., Schweizer F., Goudfrooij P., 2004, A&A, 416, 467
Matthews L. D., Gallagher J. S., 2002, ApJS, 141, 429
McDermid R., Emsellem E., Cappellari M., Kuntschner H., Bacon R., Bureau M., Copin Y., Davies R. L., Falcón-Barroso J., Ferruit P., Krajnović D., Peletier R. F., Shapiro K., Wernli F., de Zeeuw P. T., 2004, Astronomische Nachrichten, 325, 100
Mengel S., Lehnert M. D., Thatte N., Genzel R., 2002, A&A, 383, 137
Minniti D., Kissler-Patig M., Goudfrooij P., Meylan G.,

1998, AJ, 115, 121
Mulchaey J. S., Wilson A. S., Tsvetanov Z., 1996, ApJS, 102, 309
Nagar N. M., Wilson A. S., Mulchaey J. S., Gallimore J. F., 1999, ApJS, 120, 209
Noordermeer E., van der Hulst J. M., 2006, in press (paper II)
Noordermeer E., van der Hulst J. M., Sancisi R., Swaters R. A., van Albada T. S., 2005, A&A, 442, 137 (paper I)
Osterbrock D. E., Fulbright J. P., Martel A. R., Keane M. J., Trager S. C., Basri G., 1996, PASP, 108, 277
Persic M., Salucci P., 1991, ApJ, 368, 60
Persic M., Salucci P., Stel F., 1996, MNRAS, 281, 27
Pogge R. W., 1989, ApJ, 345, 730
Roberts M. S., Haynes M. P., 1994, ARA&A, 32, 115
Roberts M. S., Whitehurst R. N., 1975, ApJ, 201, 327
Roelfsema P. R., Allen R. J., 1985, A&A, 146, 213
Rogstad D. H., Lockart I. A., Wright M. C. H., 1974, ApJ, 193, 309
Rogstad D. H., Shostak G. S., 1972, ApJ, 176, 315
Roscoe D. F., 1999, A&A, 343, 788
Rubin V. C., Burstein D., Ford W. K., Thonnard N., 1985, ApJ, 289, 81
Rubin V. C., Roberts M. S., Ford W. K., 1979, ApJ, 230, 35
Saglia R. P., Sancisi R., 1988, A&A, 203, 28
Sancisi R., 1976, A&A, 53, 159
Sancisi R., 2004, in IAU Symposium 220: Dark matter in galaxies The visible matter – dark matter coupling. p. 233
Sancisi R., Allen R. J., 1979, A&A, 74, 73
Sanghera H. S., Saikia D. J., Luedke E., Spencer R. E., Foulsham P. A., Akujor C. E., Tzioumis A. K., 1995, A&A, 295, 629
Schoenmakers R. H. M., Franx M., de Zeeuw P. T., 1997, MNRAS, 292, 349
Sellwood J. A., 1996, ApJ, 473, 733
Sofue Y., 1996, ApJ, 458, 120
Sofue Y., Rubin V., 2001, ARA&A, 39, 137
Sofue Y., Tomita A., Tutui Y., Honma M., Takeda Y., 1998, PASJ, 50, 427
Sofue Y., Tutui Y., Honma M., Tomita A., Takamiya T., Koda J., Takeda Y., 1999, ApJ, 523, 136
Spekkens K., Giovanelli R., Haynes M. P., 2005, AJ, 129, 2119
Swaters R., 1999, PhD thesis, Rijksuniversiteit Groningen
Ulvestad J. S., Wilson A. S., 1984, ApJ, 285, 439
van Albada T. S., Bahcall J. N., Begeman K., Sancisi R., 1985, ApJ, 295, 305
van Albada T. S., Sancisi R., 1986, Royal Society of London Philosophical Transactions Series A, 320, 447
van der Hulst J. M., van Albada T. S., Sancisi R., 2001, in ASP Conf. Ser. 240: Gas and Galaxy Evolution The Westerbork HI Survey of Irregular and Spiral Galaxies, WHISP. p. 451
van Driel W., 1987, PhD thesis, Rijksuniversiteit Groningen
Verheijen M. A. W., 1997, PhD thesis, Rijksuniversiteit Groningen
Verheijen M. A. W., 2001, ApJ, 563, 694
Vogelaar M. G. R., Terlouw J. P., 2001, in ASP Conf. Ser. 238: Astronomical Data Analysis Software and Systems X The Evolution of GIPSY—or the Survival of an Image Processing System. p. 358
Walcher C. J., van der Marel R. P., McLaughlin D., Rix H.-W., Böker T., Häring N., Ho L. C., Sarzi M., Shields J. C., 2005, ApJ, 618, 237
Willick J. A., 1999, ApJ, 516, 47

APPENDIX A: NOTES ON INDIVIDUAL GALAXIES

UGC 624 (NGC 338) has strongly lopsided kinematics, which makes it difficult to determine the systemic velocity accurately. When the systemic velocity is left as a free parameter in the tilted ring fits, it shows a gradual decline of almost 50 km/s towards larger radii, in an attempt to symmetrize the rotation curve. The value of 4789 km/s minimizes the asymmetries in the central parts, but even then there are differences between the approaching and receding sides of the optical spectrum. On the approaching side, the rotation curve rises rapidly to a more or less flat plateau at about 285 km/s, whereas on the receding side, the rotation curve rises more gradually to a peak of approximately 310 km/s, after which it declines slowly. In the outer parts of the HI disk ($R \gtrsim 50$ kpc), the differences are even more pronounced. On the receding side, the rotation curve declines gradually, whereas it starts to rise again on the approaching side. At the outermost point, the difference between the two halves amounts to almost 100 km/s.
It seems plausible that the asymmetries in UGC 624 are caused by gravitational interaction with its neighbour, UGC 623. Note that the distribution of the neutral gas in UGC 624 is also asymmetric (cf. Paper I).
The strong asymmetries in the velocity field lead to large residual velocities with respect to the model velocity field. Additionally, they make it difficult to accurately determine the inclination of the gas disk and we were forced to use the value from the optical isophotal analysis. This all results in large uncertainties in the rotation curve, especially in the outer parts. This galaxy is therefore not suitable for a derivation of the dark matter properties and will not be used in our subsequent mass-modelling.

UGC 2487 (NGC 1167) is a giant S0 galaxy ($M_B = -21.88, D^B_{25} = 54$ kpc; see Paper II) with an extended, highly regular gas disk. We can trace the HI rotation curve out to radii of 80 kpc (10 R-band disk scale lengths) and although there is a small decline in the rotation velocities, they remain well above 300 km/s till the outermost point. The total mass enclosed within the last measured point is $M_{\rm enc} = 2.1 \cdot 10^{12}\,{\rm M}_\odot$, which makes UGC 2487 the most massive galaxy in our sample. The total enclosed mass is larger even than those in the giant Sc galaxies NGC 2916 and UGC 2885 (Rubin et al. 1979; Roelfsema & Allen 1985, note that in both papers a Hubble constant of $H_0 = 50$ km s^{-1} Mpc^{-1} is assumed; their derived masses have to be divided by 1.5 when using our value of 75 km s^{-1} Mpc^{-1}); to our knowledge, it is the largest mass ever derived from a rotation curve. Saglia & Sancisi (1988) list a number of other large disk galaxies with extremely high rotation velocities; some of those galaxies may be even more massive than UGC 2487, but since no spatially resolved rotation curves are available for these systems, no accurate values for the total masses can be derived. In any case, UGC 2487 seems member of a class of extremely massive disk galaxies (see also Giovanelli et al. 1986; Carignan et al. 1997), with masses that rival those of the most massive elliptical galaxies (e.g. Bertin et al. 1988; Minniti et al. 1998).
UGC 2487 is also classified as a Seyfert galaxy, explaining the broad emission lines in the nucleus (cf. Filippenko & Sargent 1985). It has a central compact steep spectrum (CSS) radio source (e.g. Sanghera et al. 1995; Giovannini et al. 2001), which is responsible for the HI absorption in the centre. Away from the bright nucleus, we detect some very faint emission in the optical spectrum. Although this emission seems to follow the general sense of rotation of the galaxy, the emission profiles are broad and do not have well-defined peaks. From these data alone, it is difficult to determine whether this faint emission traces regular rotation in the circumnuclear regions, or whether it is related to outflows from the active nucleus. Thus, this emission gives no useful information on the shape of the potential in the inner regions and we have decided not to use it in the derivation of the rotation curve. A small HII region is detected 30″ away from the centre on the approaching side; the emission from this region has regular line profiles and its velocity is consistent with the rotation velocities of the HI at the corresponding location.

UGC 2916 has a regular, symmetric rotation curve in its central regions. In the outer parts, however, a strong asymmetry is present between the approaching and the receding sides of the galaxy. At the approaching side, the rotation velocities show a strong increase outside the optical disk and reach a maximum of approximately 240 km/s at 20 kpc; further outwards the rotation velocities decline again. At the receding side, the rotation velocities do not rise at all outside the optical disk, but start to decline immediately. It seems likely that the lopsidedness in this galaxy is the result of the interaction with its nearby companion PGC 14370.

UGC 2953 (IC 356) is by far the best resolved galaxy in our sample, with 117 independent data points in its rotation curve. The inner points, from the optical spectrum, sample the rotation velocities at intervals of ∼80 pc or 0.02 R-band disk scale lengths, whereas the last measured point lies at a projected radius of 59 kpc (14 disk scale lengths). The central rise in the rotation curve is unresolved even in the optical spectrum; the rotation velocities rise to ∼200 km/s within 1 arcsecond from the centre, and keep rising more gradually from there to a maximum of 310 km/s at $R \approx 100''$ (≈ 7.5 kpc, 2 disk scale lengths). In the outer regions, the rotation curve declines, with the asymptotic velocity about 15% lower than the maximum. The strong variation in the fitted inclination angles around $R = 600''$ is probably an artefact caused by streaming motions in the large spiral arm in the western parts of the galaxy; it was not judged to be real and was therefore not used in the final tilted ring fits.

UGC 3205 has one of the most symmetric HI disks of all galaxies in our sample, both in its morphological appearance (see Paper I) and in its kinematics. The optical image is highly regular as well (Paper II). There is an almost perfect symmetry in the velocity field, and the rotation curves for the approaching and receding sides of the galaxy are identical within the measurement errors. The residual velocities are small too; the only significant residuals are detected in the regions where the bar causes non-circular streaming motions. It seems plausible that such streaming motions are also responsible for the apparent variation in inclination angle in the central parts; we find it unlikely that the fitted variation is real and have assumed a constant value for the final tilted ring fits. Outside the bar region, the residual velocities are of order 10 km/s or less everywhere, indicating

that the gas motion is highly regular and undisturbed.
In the centre of the optical spectrum, a peculiar offset is detected between the centre of symmetry of the rotation curve and the centre of the continuum emission; the former is shifted by about one arcsecond ($\sim$ 250 pc) to the south-west with respect to the latter. It seems unlikely that this offset is caused by absorption of light by dust (as is most likely the case in UGC 3580), as the optical image is highly symmetric and shows no signs of dust extinction whatsoever. No other peculiarities are seen in this galaxy at all and the origin of the offset remains unclear to us. For the derivation of the optical rotation curve, we have used the centre of symmetry of the line emission, rather than the continuum centre, to fold the two halves onto each other. Given the flatness of the rotation curve and the high degree of symmetry at larger radii in the spectrum, a different choice for the dynamical centre would not have led to significantly different rotation velocities, except for the very inner points.
The resulting rotation curve of this galaxy seems to lack, almost completely, the characteristic steep rise in the centre which is observed in most other galaxies in our sample. Parts of the central regions are devoid of gas though, and we cannot trace the entire rise of the rotation curve.

UGC 3546 (NGC 2273) is classified as a Seyfert galaxy (Huchra et al. 1982). High-resolution observations with the VLA revealed a bright radio continuum source in the centre, consisting of two separate lobes separated by about 0.9″ or $\approx$120 pc (Ulvestad & Wilson 1984; Nagar et al. 1999). The optical spectrum shows strong nuclear emission lines, the nature of which has been discussed by Ho et al. (1997). The Hα emission in our optical spectrum is clearly extended (cf. Pogge 1989; Mulchaey et al. 1996), but the line profiles are irregular and broad out to a radius of about 10″; within this radius, it is difficult to disentangle the effects of quiescent rotation from possible in- and outflows from the nucleus. The uncertainties in the inner points of the rotation curve are therefore large, and the sharp peak and subsequent decline in the rotation curve may not be real.
In contrast, the HI velocity field displays smooth and regular rotation throughout the entire gas disk of the galaxy. The central part of the velocity field appears somewhat distorted, but this is an artefact caused by beam smearing (see also Paper I). This also explains the erratic behaviour of the fitted orientation angles in the inner regions; for the final tilted ring fits, we have used the position angle and inclination determined from larger radii, as indicated with the bold lines in the figures in appendix C. No effects can be seen of non-circular motion in the bar, possibly due to its favourable orientation (perpendicular to the major axis).

The centre of symmetry in the optical spectrum of **UGC 3580** has an offset of approximately one arcsecond ($\sim$100 pc) with respect to the peak in the continuum emission (indicated with the dashed line in the figure in appendix C). This difference is most likely caused by obscuration of the continuum emission by dust. As was noted in Paper II, the optical image shows strong dust features in the central regions of this galaxy. Thus, a determination of the centre of the galaxy based on the peak in the light distribution is problematic and it is not surprising that the dynamical centre is offset with respect to the isophotal one. Not only the optical appearance of this galaxy is peculiar, the kinematical structure is remarkably different from that of most galaxies in our sample as well. There is a marked asymmetry between the approaching and receding sides of the optical spectrum. Whether this reflects a true lopsided kinematics in the central regions or is a result of dust extinction too, is difficult to determine from these data alone. The major axis slice through the HI data cube is also asymmetric, but it appears that this asymmetry is peculiar to the major axis; it does not occur equally strong at different position angles and the rotation curves averaged over the full halves of the velocity field are only marginally different. Similarly to other galaxies in our sample, the central rise of the rotation curve of UGC 3580 is steep. But where in most of our galaxies the rotation curve becomes flat after the initial rise, or even starts to decline, it continues to rise gradually till twice the optical diameter ($\sim$8.5 R-band disk scale lengths) in this galaxy and only flattens out at the edge of the gas disk. This behaviour resembles that of typical late-type and dwarf galaxies (Broeils 1992; Swaters 1999) which generally have slowly rising rotation curves too. However, although UGC 3580 is one of the least luminous galaxies in our sample ($M_{\rm B} = -18.31$) and correspondingly has one of the lowest maximum rotation velocities ($V_{\rm max} = 127$ km/s), its luminosity is still too high to classify it as a dwarf galaxy. UGC 3580 thus seems to be a relatively luminous member of a class of low-luminosity early-type disk galaxies which have distinctly different morphological and kinematical features compared with their high-luminosity counterparts; other nice examples of this class are UGC 6742, UGC 12043 and UGC 12713 (see Paper I).

UGC 3993 is an S0 galaxy with a regularly rotating gas disk. It resembles UGC 2487, but it is not as large nor as massive. Although the galaxy is quite face-on, the HI velocity field is of sufficient quality to determine the inclination with reasonable accuracy. Nevertheless, the uncertainties in the rotation velocities due to the inclination errors are large. In particular, we cannot exclude the possibility that the decline in the rotation curve of this galaxy is caused by a small warp in the outer parts towards a more face-on orientation.

The rotation curve of **UGC 4458** (NGC 2599) looks remarkably different from the canonical flat rotation curves normally observed in spiral galaxies. Instead, it rises very rapidly to an extreme peak velocity of 490 km/s, after which it shows a sharp decline of more than 50% before it asymptotically approaches a constant rotation velocity of $\sim$240 km/s. The central rise in the rotation curve is unresolved even in our optical spectrum; it is possible that in the very inner regions, gas moves at even higher rotation velocities. Already, a rotation velocity of 490 km/s is unusually high, and seems surpassed only by that of UGC 12591 (Giovanelli et al. 1986).
UGC 4458 is, however, close to face-on and the errors in the rotation velocities, caused by the uncertainties in the exact value of the inclination, are large. Thus, the peak velocity could be substantially lower if the galaxy were slightly more inclined in the inner parts, and the extreme decline in the rotation curve could partly be explained by a small warp towards a more face-on orientation in the outer parts. To fully explain the decline as a result of a warped gas disk, however, the inclination would have to decrease steadily from 31° in the centre to 15° in the outer parts (assuming a constant

rotation velocity of 400 km/s). Such a change in inclination angle is not detected in the tilted ring fits, and it seems unlikely that the decline in the rotation curve can be explained fully by warping of the gas disk. Meanwhile, we cannot exclude a small warp towards a higher inclination in the outer regions either. In particular, our data are also consistent with a continuing, Keplerian decline in the outer points of the rotation curve, and thus, with an absence of dark matter inside the radii probed by the HI disk. We will investigate this issue in more detail in our subsequent paper on the mass modelling.

The central parts of the gas disk of **UGC 4605** (NGC 2654) are close to edge-on, with an estimated inclination angle of 84°. At larger radii, the gas disk warps towards a more face-on orientation. Due to the high inclination and the resulting line-of-sight integration effects, the central regions of the velocity field have a bias towards the systemic velocity and do not give an accurate representation of the projected rotational velocities (see also Paper I), so the usual tilted ring analysis could not be used there. Within a radius of $R = 30''$, this problem could be circumvented by using the optical spectrum; due to its higher spatial resolution, it suffers much less from projection effects. Between $R = 30''$ and $R = 110''$, where no optical information is available, we determined the rotation velocities by hand from the HI data, using the same method that was normally used for the inner regions of the optical spectra (section 3.2). At each position along the major axis, the terminal velocity of the line profile was determined and assumed to represent the projected rotational velocity at the line of nodes; the average of the rotation velocities for the approaching and receding sides of the galaxy was then taken as the true rotation velocity at that radius. Outside $R = 110''$, the gas disk becomes sufficiently less inclined that tilted ring fits could be applied to the velocity field; the rotation curve for $R > 110''$ was therefore determined in the usual way.
The edge-on orientation of this galaxy also has a positive effect, namely that the uncertainties in the inclination angle are small; the resulting errors in the rotation velocities are almost negligible.
The final rotation curve is well defined and symmetric, except for the region around $120''$, where the rotation velocities on the approaching side are declining already while those on the receding side are still constant. Beyond this region, the rotation curve is symmetric and shows a strong decline on both sides. At larger radii ($R \gtrsim 200''$), the rotation curve flattens out at a level of approximately 185 km/s.
Due to the edge-on orientation of this galaxy, no accurate optical photometry could be obtained and we were only able to obtain an estimate for the radial scale length of the stellar disk. But the rotation curve is relatively flat between 2 and 3 times the estimated scale length, so the value for $V_{2.2h}$ is reasonably robust. Due to the lack of detailed information on the stellar mass distribution, however, this galaxy can not be used for mass modelling.

The outer parts of the gas disk of **UGC 5253** (NGC 2985) are dominated by a large spiral arm extending from the north of the galaxy. Although the gas in the arm is clearly rotating, it is impossible to determine the exact orientation of the arm and we have only fitted a tilted ring model to the inner parts. Even so, our rotation curve extends out to a radius of 49 kpc, or ∼9 R-band disk scale lengths.
The most interesting aspect of UGC 5253, however, is the strong m=0 component in the residual velocity field. Both in the inner ($R \lesssim 200''$) and in the outer ($R \gtrsim 400''$) regions, the residual velocities are small, indicating that our fitted tilted ring model is an accurate description of the observed gas motions. Around a radius of $300''(\approx 30\text{kpc})$, however, a ring-like feature is detected in the residual field with an amplitude of -20 km/s. This feature has a high degree of symmetry with respect to the centre of the galaxy and the residual velocities are almost constant with position angle; only at the western end of the ring are the residuals slightly lower (~ -10 km/s). In the rotation curve, the feature manifests itself as a marked asymmetry between the approaching and receding side. However, simple kinematical asymmetries can only explain residuals along the major axis of a galaxy; without additional radial motions, they must always vanish on the minor axis. The fact that the residual velocities in the ring are so symmetric and also present on the minor axis, argues against a simple explanation in terms of a kinematical asymmetry.
A more plausible explanation of the marked m=0 component in the residual field is that it is induced by the gravitational perturbations from the large spiral arm in the outer parts. It was shown by Schoenmakers et al. (1997) on theoretical grounds that an m=1 perturbation in the gravitational potential leads to a strong m=0 term in the residual velocity field. The combination of the large m=1 spiral arm in the gas distribution of UGC 5253 and the pronounced m=0 term in its residual field are thus a strong empirical confirmation of their predictions. Furthermore, Schoenmakers et al. (1997) showed that it is, in principle, possible to use the amplitude of the m=0 term in the residual field to measure the strength of the perturbation on the potential. This analysis is, however, beyond the scope of this paper and will be postponed to a later time.
Alternatively, we could be seeing a vertical vibrational mode in the gas disk of UGC 5253, where the entire ring is moving upwards (i.e. towards us) with respect to the rest of the galaxy. Sellwood (1996) and Edelsohn & Elmegreen (1997) showed the results of N-body simulations which suggest that vertical vibrations can exist in the disks of galaxies, possibly triggered by a tidal interaction with a companion galaxy. It seems, however, questionable if such a mechanism could explain the highly symmetric feature we observe in UGC 5253, and we judge the explanation of Schoenmakers et al. (1997) more plausible.
Note that the feature in the residual field coincides with a marked drop in the rotation curve. Both inside $R = 200''$ and outside $R = 400''$, the rotation curve is flat, but around $R = 300''$, it suddenly drops from 245 to 210 km/s; the rate of the decline is consistent with pure Keplerian decay. Whether it is a coincidence that this drop occurs at similar radii as the feature in the residual field, or whether both effects are related, is unclear.

A strong stellar Hα absorption feature is present in the central arcseconds of the optical spectrum of **UGC 6786** (NGC 3900); no Hα emission is detected in the inner parts. Emission *is* detected in the central parts in the 6583.46 Å [NII] line, but the standard procedure of stacking together the different emission lines in the optical spectrum cannot

be used here. Instead, we analysed the Hα and [NII] lines separately in this case, and combined the resulting rotation curves afterwards; at positions where emission was detected in both lines, the average velocity was calculated. The spectrum shown in the figure in appendix C was created by replacing the inner part (15 pixels on either side of the centre) of the Hα spectrum by the corresponding region of the [NII] line. Thus, it shows the extended Hα emission in the outer regions, together with the [NII] emission in the nuclear region.
Note that the central emission in the [NII] line is irregular, with broad line profiles. This may be explained as a result of line-of-sight integration effects through the inner regions of the massive bulge of UGC 6786 (see Paper II), but observations at higher spatial resolution and sensitivity are required to investigate this in more detail. At a radius of $5''$ on the approaching side, a strong emission feature is detected which has a velocity that lies more than 100 km/s closer to the systemic velocity than the emission at smaller radii. It seems unphysical that this emission traces regular rotation of gas in the plane of the galaxy and we did not include it in the combined rotation curve.
The outer parts of the HI disk are distorted as well, with two large spiral arms extending from the symmetric inner disk. It is impossible to determine the exact orientation of the gas in these arms and no tilted rings were fit outside a radius of $240''$. The residual velocity field shows a peculiar m=5 harmonic component in the azimuthal direction. According to the results of Schoenmakers et al. (1997), this implies an m=6 perturbation in the gravitational potential of this galaxy. No obvious source of such a perturbation can be identified in the visible matter in this galaxy, so the perturbation, if real, must be caused by the dark matter halo. Since UGC 6786 does not have a regular exponential stellar disk, no disk scale lengths are indicated in the figures in appendix C.

The rotation curve of **UGC 6787** (NGC 3898) is well resolved and shows some characteristic 'wiggles' with an amplitude of 30 – 50 km/s. The kinematics in the central parts are only barely resolved in the optical spectrum, and due to the high inclination angle and resulting line-of-sight integration effects, the central line-profiles are strongly broadened. After the initial rise of the rotation curve to the peak velocity of 270 km/s, the rotation velocities drop to approximately 220 km/s at a radius of $30''$ (~ 2.75 kpc), after which they gradually rise again to 250 km/s at $R \approx 100''$ (~ 9 kpc). The rotation velocities then drop again to 220 km/s, after which they rise again to reach a more or less flat plateau at 250 km/s. Although there are clear indications that the gas disk of UGC 6787 is warped, the locations of the 'wiggles' in the rotation curve do not coincide with the radii where the position angle and the inclination change and the variations in the rotation velocity seem real. This is further confirmed by the fact that the variations occur symmetrically at all position angles over the velocity field.
The discrepancy between the kinematic inclination angle derived here and the optical inclination from Paper II can be explained by the dominance of the bulge in the optical image. As was noted in Paper II, the optical image of this galaxy is dominated by the spheroidal bulge out to large radii, which makes it impossible to obtain a reliable estimate for the inclination from the isophotes. The kinematical inclination derived here is free of such effects and thus reflects the true orientation of this galaxy more accurately.

UGC 8699 (NGC 5289) is highly inclined and the central line profiles in the optical spectrum are severely broadened by the combined effect of beam smearing and line-of-sight integration effects. Similar to UGC 6787, the rotation curve of this galaxy shows a distinct 'bump'. After an initial rise, the rotation curve reaches a peak velocity of 205 km/s at a radius of approximately $8''$(≈ 1.4 kpc). At $R \approx 30''$ (≈ 5.5 kpc), the rotation velocities have fallen to 170 km/s, but unfortunately, no Hα emission is detected between 15 and $30''$ on either side of the galaxy, so the exact shape of the decline in the rotation curve cannot be recovered. Between $R = 30''$ and $R = 45''$, the rotation curve rises back to approximately 200 km/s, symmetrically on both sides of the galaxy. At the approaching side of the optical spectrum, no emission is detected anymore beyond this radius; at the receding side, the spectrum indicates a small decline again in the rotation velocities, out to the last measured point at $54''$(≈ 9.7 kpc).
In the HI observations, UGC 8699 is poorly resolved along the minor axis. Comparison of the xv-slice through the HI data cube with the optical spectrum shows that there is probably a central hole in the HI disk, explaining the absence of HI emission at high rotation velocities close to the centre. Thus, this galaxy provides another good illustration of the use of the optical observations to resolve the shape of the inner rotation curve. Because of the poor resolution along the minor axis, standard tilted ring fits did not recover the rotation velocities accurately in this case. Instead, we used only points close to the major axis to determine the HI rotation curve; points within 60° of the minor axis were discarded in the fits. In the outer parts, a small asymmetry is detected between the rotation velocities of the approaching and receding sides of the galaxy, with the former rotating about 10% slower than the latter.

UGC 9133 (NGC 5533) has the most extended rotation curve in our sample, with the outermost point in the rotation curve lying at a projected radius of 103 kpc (> 11 R-band disk scale lengths). With a rotation velocity at this radius of 225 km/s, the total enclosed mass is $1.3 \cdot 10^{12}\,\mathrm{M}_\odot$. Most gas at large radii lies in a giant spiral arm which extends from the north-east side of the gas disk and is warped with respect to the inner parts of the galaxy. Although the arm is clearly rotating and the fitted position and inclination angles are well-behaved, the lack of symmetry in the arm makes it difficult to exclude the possibility that the gas in the arm is not rotating at perfectly circular orbits. Therefore, care should be taken with the rotation velocities outside R $\approx 200''$. Note, however, that we have assumed rather conservative values for the uncertainty Δi in the inclinations, such that the corresponding uncertainties ΔV_i in the rotation curve (indicated with the shaded area in the figures in appendix C) also include, at least partly, the uncertainties introduced by the orientation of the spiral arm. Note also that the residual velocities with respect to the tilted ring model are small, indicating that the non-circular motions are not dominant.
The optical observations do not have sufficient resolution to trace the rise of the rotation velocities in the centre. Furthermore, a bright central component complicates the inter-

pretation of the spectrum in the inner few arcseconds (see also appendix B). At larger radii, however, the spectrum is highly regular and symmetric.
The rotation curve of UGC 9133 keeps declining almost to the outermost points in the HI rotation curve. The asymptotic velocity is about 25% lower than the maximum. Only at a radius of approximately 80 kpc does the rotation curve flatten out.

UGC 11670 (NGC 7013) has a giant bar; the large 'wiggle' in the rotation curve around R = 50″ may well be an artefact caused by streaming motions in this bar. The change in position angle which is detected at those radii is most likely also caused by non-circular motions and for the final rotation curve, we assumed that the position angle is constant at -24° in the inner regions. At larger radii, the rotation curve becomes smoother and shows a gradual decline out to a radius of about 300″(18 kpc), after which the rotation velocities seem to rise again. The upturn is only visible in the low-resolution data, but seems to occur on both sides of the galaxy, which strengthens the detection. We can, however, not exclude the possibility of in- and outflows in the outer parts of the gas disk of this galaxy; deeper observations are needed to verify if the gas in the outer parts is truly on circular orbits and if the rise in the rotation curve is real.
In the centre, a bright nuclear component complicates the interpretation of the optical spectrum (see appendix B) and the inner points of the rotation curve may not be reliable.

UGC 11852 has the most extended gas disk, relative to the optical size, of all galaxies in our sample. It allows us to trace the rotation curve to a radius of ∼90 kpc, or ∼21 R-band disk scale lengths. This galaxy is clearly warped: the fitted position angles from the tilted ring fits change by more than 20° from the inner to the outer parts of the disk. The inclination changes as well and the galaxy becomes more edge-on in the outer parts. The apparent variation in the fitted inclinations in the inner regions is probably an artefact caused by non-circular motions in and around the bar; it is not included in the final fit. The rotation curve can be seen to rise steeply in the inner regions, although the exact shape of the inner rotation curve cannot be recovered due to the strong central component present in the optical spectrum (see also appendix B). Outside the optical disk, the rotation curve shows a marked decline, but it seems to flatten out in the outer parts. The asymptotic rotation velocity is approximately 25% lower than the maximum. Strong residual velocities (up to −50 km/s) are detected northwest of the centre of the galaxy. The velocities of the gas in this region are incompatible with regular rotation and indicate large-scale streaming motions.

UGC 11914 (NGC 7217) has a highly regular gas disk; the rotation curves of the approaching and receding sides separately are almost indistinguishable. Unfortunately, however, the inclination is not tightly constrained and the resulting uncertainties in the rotation curve are large.
Comparison of this galaxy with similar systems in our sample (e.g. figures 4 – 6) implies that it should have a declining rotation curve. The fact that we do not see such a decline is probably caused by the small radial extent of the HI disk, which enabled us to measure the rotation curve out to 3.3 R-band disk scale lengths only. In several other galaxies in our sample (e.g. UGC 2487, 5253), the decline in rotation velocities sets in around the edge of the optical disks, and it does not seem unreasonable to assume that the rotation curve of UGC 11914 declines at similar radii.
Due to its relative proximity, UGC 11914 is one of the few galaxies where we fully resolve the inner rise of the rotation curve in the optical spectrum. We clearly see the gradual change in velocity from the approaching to the receding side over the central 30″. Superposed over the 'normal' emission, we detect the bright and unresolved central LINER component (cf. Keel 1983). The line profile of the LINER is very broad and implies velocities well in excess of the quiescent rotation velocities at larger radii (see also appendix B).

UGC 12043 (NGC 7286) is the least luminous galaxy in our rotation curve sample and the amplitude of the rotation curve is correspondingly low ($V_{\rm max} = 95\,$km/s). In contrast, the rotation curve is the second most extended, compared to the optical size, of all galaxies in our sample, with the outermost point lying at a projected radius almost 19 times larger than the R-band disk scale length. This galaxy is the only case in our sample with a slowly rising rotation curve. It completely lacks the steep central rise observed in all other galaxies in our sample and, instead, rises gradually to the maximum which is only reached around 3 optical scale lengths. This behaviour can be explained by the fact that UGC 12043 has no bulge and thus has a much smaller central surface density than all other galaxies in our sample (see Paper II). UGC 12043 is thus a member of a class of low-luminosity early-type disk galaxies which have distinctly different morphological and kinematical features than their high-luminosity counterparts; other nice examples of this class are UGC 3580, UGC 6742, and UGC 12713 (see Paper I).
The interpretation of the optical spectrum is complicated by the low spectral resolution of the GoldCam spectrograph used for these observations. Although the rotation of the galaxy can clearly be detected, the line profiles are practically unresolved and no corrections can be made for beam smearing or line-of-sight integration effects. A sudden jump occurs in the receding side of the optical spectrum, around R=20″, the nature of which is unclear; no emission is detected at the corresponding radius on the approaching side.
The HI velocity field is highly symmetric, and the inferred rotation curves for the approaching and receding sides separately are virtually indistinguishable, except for the outer parts of the low-resolution velocity field (not shown in the figure in appendix C), where the approaching side exhibits a sudden rise in the rotation velocity. This rise is probably caused by non-circular motions in the outer disk of the galaxy and most likely does not correspond to a real increase in the rotation velocity; it is not included in the final, azimuthally averaged rotation curve.

APPENDIX B: BROAD CENTRAL VELOCITY PROFILES IN THE OPTICAL SPECTRA

In about half of the galaxies in our sample, broad velocity profiles are present in the optical spectra of the central regions; the velocity amplitudes of those features often exceed the rotational velocities observed at larger radii. In some cases, especially in the Seyferts UGC 2487 and 3546, these

Table B1. Central features in the optical spectra. (1) UGC number; (2) central velocity of line profile; (3) profile width, measured at 20% of the maximum flux; (4) derived rotational velocity; (5) estimated diameter; (6) total enclosed mass; (7) average density within D_c; (8) total R-band luminosity within D_c and (9) R-band mass-to-light ratio within D_c.

UGC	V_0	W_c	V_c	D_c		M_c	ρ_c	$L_{c,R}$	$(M/L)_{c,R}$
	km/s	km/s	km/s	$''$	kpc	$10^9\,M_\odot$	$10^3\,\frac{M_\odot}{pc^3}$	$10^8\,L_\odot$	$M_\odot/L_\odot$
(1)	(2)	(3)	(4)	(5)		(6)	(7)	(8)	(9)
2487	– Seyfert nucleus –								
2953	911	470	307	1.1	0.08	0.86	3.4	0.34	25
3546	– Seyfert nucleus –								
5253	1324	317	263	1.1	0.11	0.88	1.3	1.3	7
8699	2553	434	227	1.1	0.20	1.2	0.28	0.58	21
9133	3860	490	307	1.5	0.40	4.4	0.13	5.7	8
11670	781	357	190	2.6	0.16	0.69	0.30	0.96	7
11852	5851	355	232	1.9	0.74	4.6	0.022	4.5	10
11914	947	472	458	1.1	0.08	2.0	6.9	0.42	48

broad components may be explained as a result of nuclear activity and related gas flows. In the other cases, however, no strong nuclear activity is observed and the most natural explanation of the observed velocities is a nuclear disk or ring, possibly rotating around a massive nuclear star cluster or super-massive black hole. Similar rapidly rotating components have been observed in the centers of many other spiral galaxies (e.g. Carter & Jenkins 1993; Bertola et al. 1998; Sofue et al. 1998, 1999; Sofue & Rubin 2001 and references therein; McDermid et al. 2004; Fathi 2004), and may well be the spectroscopic counterparts to the nuclear structures imaged by e.g. Carollo et al. (1997, 1998).

In most cases, the central structures are spatially unresolved in our spectra, but in a few cases (e.g. UGC 11670, 11852) the resolution is sufficient to detect a velocity gradient. These gradients are always in the same direction as the sense of rotation of the gas at larger radii, which further strengthens our assumption that the central features in the spectra originate from regularly rotating gas.

The data presented here lack the spatial resolution to unambiguously determine the nature of the central components in our spectra. A proper investigation would require sub-arcsecond resolution, both for the kinematic as for the photometric data, i.e. either space-based or adaptive-optics assisted observations. A nice example of the potential of such observations was recently presented by Atkinson et al. (2005), who used imaging and long-slit spectroscopy from the Hubble Space Telescope to derive limits on the mass of the central black holes in NGC 1300 and 2748 (see also Harms et al. 1994; Ferrarese & Ford 1999).

With our data, we can only estimate the total mass in the central regions of our galaxies. The results of our crude analysis are summarized in table B1. The rotational velocities of the gas were derived from the width W_c of the central line profiles, measured at 20% of the maximum flux, assuming that the central gas has the same orientation as the outer disk: $V_c = W_c/(2\sin i)$. Note that the true rotational velocities may be larger or smaller if the central disks are tilted with respect to the main disk for which we derived the inclination angle, or if significant non-circular motions are present. The total extent of the gas in the central component was estimated by eye from the spectra directly; table B1 gives the estimated diameters D_c. In most cases, the resolution of our data allows us to probe diameters of a few hundred parsecs or less; for the distant galaxy UGC 11852, the constraints are somewhat worse. Since in all cases, the structures are not or only marginally resolved, the diameters given in table B1 are highly uncertain and, strictly speaking, upper limits only. Finally, if we make the additional assumption that the central mass concentration has a spherically symmetric shape, the total enclosed mass can be estimated using equation 1.

Table B1 clearly shows that the inferred central masses and densities are high, especially in the nearby galaxies where we have better constraints on the total extent of the rapidly rotating gas. Central densities of order $10^3\,M_\odot\,pc^{-3}$ and higher can almost certainly not be explained by the normal stellar components. In column (8) of table B1, we give the total R-band luminosities within D_c, as measured from the optical images presented in Paper II. It is clear that the observed luminosities are too small to account for the derived dynamical masses; the local mass-to-light ratios are much larger than what is expected for the surrounding bulge material.

Our inferred masses are also a few orders of magnitudes larger than those of the most massive stellar clusters known to date (e.g. Mengel et al. 2002; Maraston et al. 2004; Walcher et al. 2005), so it is unlikely that the high rotation velocities are caused by unresolved central concentrations of stars. For UGC 2953, 5253, 11670 and 11914, HST images are available (e.g. Carollo et al. 2002; Hunt & Malkan 2004) and we could explicitly verify that no bright and compact sources of light are hidden in our own, lower-resolution images.

In conclusion, the central components in our spectra seem to be a strong indication for the presence of supermassive black holes in at least a fraction of our galaxies. Sub-arcsecond observations, however, are required to obtain more detailed knowledge on the spatial extent and orientation of the rapidly rotating gas and to provide conclusive evidence for the presence and mass of the black holes.

APPENDIX C: ROTATION CURVES

On the following pages, we present the rotation curves and several other related quantities for all galaxies in the sample. For each galaxy, we show a figure consisting of the following panels:

Left hand column: velocity fields
Top: grayscale and contour representation of the observed HI velocity field from Paper I. Darker shading and white contours indicate the receding side of the galaxy. Contours are spaced at intervals of 25 km/s; the thick contour indicates the systemic velocity from table 2.
Middle: model velocity field, based on the tilted ring fits to the velocity field shown above. Contours and grayscales are the same as in the observed velocity field.
Bottom: Residual velocity field, produced by subtracting the model velocity field from the observed one. The grayscales range from -40 to +40 km/s (white to black). Contours are spaced at intervals of 25 km/s; the thick contour indicates zero residual velocity.
The cross in each panel indicates the dynamical centre, as given in table 2.

Top row: x-v diagrams
Middle: cleaned and stacked optical spectrum (see section 3.2.2 for a description of how these were produced).
Right: major axis position-velocity slice through the HI data cube.
The position angles on the sky of both plots are indicated in the top left corner of the panels. Contours in both panels are at -1.5 and -3 (dotted) and $1.5, 3, 6, 12, \ldots$ times the rms noise in the respective datasets. The dashed horizontal and vertical lines denote the systemic velocity and the centre of the galaxy respectively. The fitted rotation velocities are overplotted. For each of the two sides of the plots, approaching and receding, we plot the velocities derived from fits to that side only. Plotting symbols are as follows:
– blue/black squares show velocities derived from the final tilted ring fits to the HI velocity fields;
– red/dark gray bullets show velocities fitted to the optical line profiles.
– orange/light gray bullets show the central locations in the optical spectra which were affected by 'optical beam-smearing' and where the rotational velocities were determined by eye, rather than by Gaussian fits (see section 3.2.4).

Bottom row, middle panels: Orientation parameters from the tilted ring fits to the HI velocity fields.
Top: data points show the fitted position angles (north through east) from fits with position and inclination angle left free. The bold lines give the values that were used for the final fits to derive the rotation curves. The arrows give the values derived in Paper II from the outer isophotes of the optical image.
Bottom: data points show the fitted inclination angles from fits with inclination angle left free and position angle fixed at the values shown with the bold line in the top panels. The bold lines give the values for the inclination angle that were used for the final fits to derive the rotation curves; the shaded regions show the adopted uncertainties. The arrows give the values derived from the outer isophotes of the optical image.

Bottom row, right hand panels: Rotation curves.
Left: inner regions.
Right: full rotation curves.
The axes at the bottom show radii in arcseconds, those at the top show the corresponding radii in kiloparsecs.
Plotting symbols and linestyles are as follows:
– filled blue/black squares show velocities derived from the final tilted ring fits to the HI velocity fields; the position and inclination angles assumed for these final fits are indicated with the bold lines in the middle panels of the bottom row.
– open blue/black squares show velocities that were derived from HI data at lower resolution than those shown in the left column and top row.
– red/dark gray bullets show the velocities from the optical spectra.
– orange/light gray bullets show optical velocities that were manually adapted to correct for beam-smearing and line-of-sight integration effects in the optical spectra (see section 3.2.4).
– crosses and plus-signs indicate the rotation curves for the approaching and receding sides respectively.
– errorbars are a combination of fitting errors and differences between the approaching and receding sides (see section 3.4).
– bold lines show the smoothed rotation curves, derived from cubic spline fits through the individual data points (see section 3.3 for details).
– dashed lines indicate regions where no optical emission was detected.
– shaded regions show the uncertainties in the rotational velocities due to the adopted uncertainties in the inclination; for clarity, they are drawn around the smoothed rotation curve, rather than around the individual data points.
– vertical arrows at the bottom show the radii corresponding to one (left) and two (right) disk scale lengths of the R-band image (see Paper II); horizontal arrows at the right show the derived maximum and asymptotic rotation velocities and the rotation velocity at 2.2 R-band disk scale lengths (see table 2).

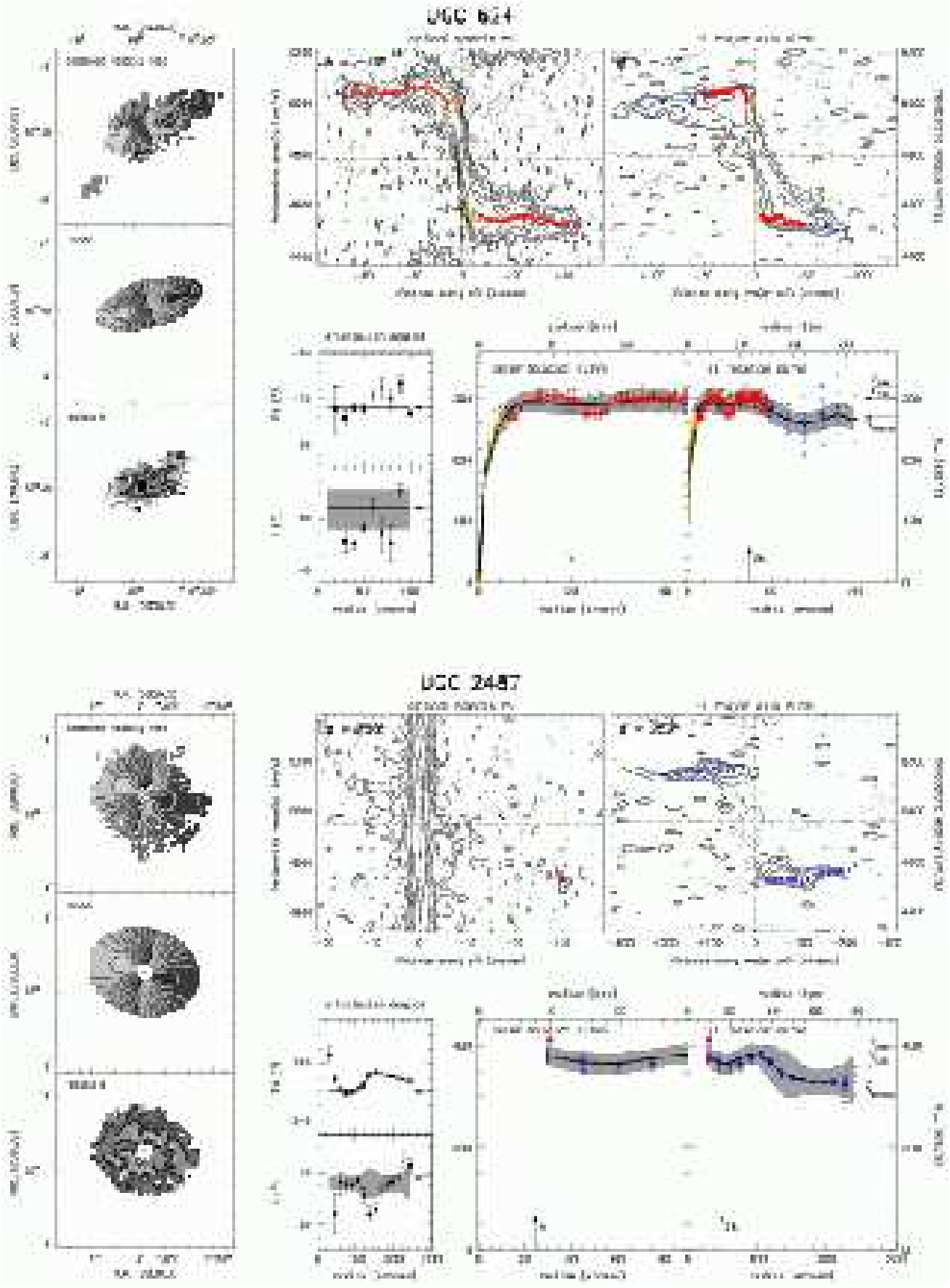
UGC 624
UGC 2487